
Ambient Dataloops: Generative Models for Dataset Refinement

Adrian Rodriguez-Munoz

Massachusetts Institute of Technology
adrianrm@mit.edu

William Daspit

The University of Texas at Austin
wdaspit@utexas.edu

Adam Klivans

The University of Texas at Austin
klivans@utexas.edu

Antonio Torralba

Massachusetts Institute of Technology
torralba@mit.edu

Constantinos Daskalakis

Massachusetts Institute of Technology
costis@csail.mit.edu

Giannis Daras

Massachusetts Institute of Technology
gdaras@mit.edu

Abstract

We propose Ambient Dataloops, an iterative framework for refining datasets that makes it easier for diffusion models to learn the underlying data distribution. Modern datasets contain samples of highly varying quality, and training directly on such heterogeneous data often yields suboptimal models. We propose a dataset-model co-evolution process; at each iteration of our method, the dataset becomes progressively higher quality, and the model improves accordingly. To avoid destructive self-consuming loops, at each generation, we treat the synthetically improved samples as noisy, but at a slightly lower noisy level than the previous iteration, and we use Ambient Diffusion techniques for learning under corruption. Empirically, Ambient Dataloops achieve state-of-the-art performance in unconditional and text-conditional image generation and *de novo* protein design. We further provide a theoretical justification for the proposed framework that captures the benefits of the data looping procedure.

1 Introduction

Much of the recent progress in generative modeling is attributed to the existence of large-scale, high-quality datasets. Indeed, modern generative models have an appetite for data that is becoming increasingly hard to fulfill (Goyal et al., 2024; Kaplan et al., 2020; Saharia et al., 2022; Hoffmann et al., 2022; Henighan et al., 2020). That triggers the formation of datasets that include any points that are available for training, including synthetic and out-of-distribution data, and naturally, these datasets contain samples of various qualities. The lower-quality parts of the training data are often removed through various filtering techniques (Gadre et al., 2023; Li et al., 2024), either from the beginning of the training or in some intermediate training stage (Sehwag et al., 2025). This approach is optimal when the bottleneck is the computational budget for training, since it is better to allocate the limited compute to the higher-quality training points (Goyal et al., 2024; Hoffmann et al., 2022). However, when the issue is not computational budget, but availability of data, filtering increases quality but comes at the cost of reduced diversity in the generated outputs (Somepalli et al., 2023a,b; Daras et al., 2024; Prabhudesai et al., 2025; Carlini et al., 2023)

Post-training, diffusion generative models often undergo refinements of all sorts to sample faster (Salimans & Ho, 2022; Song et al., 2023), become aligned with reward models (Domingo-Enrich et al., 2024; Black et al., 2023), or reduce their parameter count (Meng et al., 2023). The



Figure 1: **Dataset and model evolution across loops of our method.** D_0 shows synthetically generated images from DiffusionDB (Wang et al., 2022), a dataset used for text-to-image generative modeling. These images have artifacts due to learning errors of the underlying model. We train a model on this dataset, M_1 , that we use to improve its own training set, leading to a “restored” dataset D_1 . Successive iterations of this process lead to a co-evolution of both the model and the dataset – see dataset D_2 and model M_1 respectively. We avoid catastrophic self-consuming loops by accounting for learning errors at each iteration using Ambient Diffusion (Daras et al., 2025c, 2023) techniques for learning from imperfect data.

noisy dataset that was used to train the model remains, on the contrary, static. We hence ask: *Is it possible to use a model trained on a noisy set to improve the set that it was trained on?*

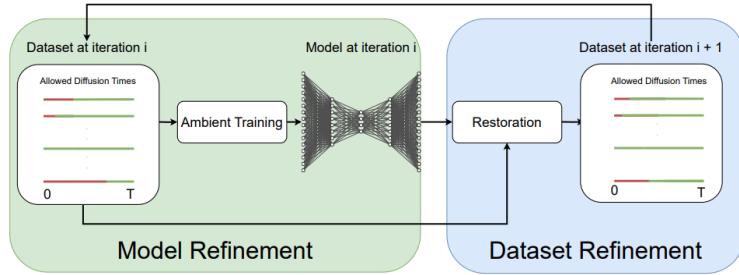


Figure 2: **Illustration of the Ambient Dataloops framework.** At each loop, we are given points that can be used to train the diffusion model at certain noise levels. We train a model on this noisy dataset using Ambient Diffusion (green), and then we use it to improve the dataset through posterior sampling (blue).

We propose a dataset-model co-evolution process, termed **Ambient Dataloops**. At each iteration of this process, we start with a noisy dataset, we use it to train a diffusion model, and then we use the trained model to **gradually** denoise the original dataset. We illustrate some results of this process for a text-conditional model in Figure 1. The concept of iterative dataset refinement has appeared in other contexts in the sampling from generative models literature (Akhound-Sadegh et al., 2024; Woo & Ahn, 2024; Denker et al., 2025). For example, the authors of (Woo & Ahn, 2024) use this idea to sample from unnormalized densities while the authors of (Denker et al., 2025) use it to sample from tilted measures using a reward model. In our work, we iteratively denoise a given noisy dataset by co-evolving the model being trained and the samples it is trained on. In our work, we iteratively denoise a given noisy dataset by co-evolving the model being trained and the samples it is trained on. We avoid catastrophic, self-consuming loops, observed in prior works (Alemohammad et al., 2024a; Shumailov et al., 2024; Hataya et al., 2023; Martínez et al., 2023; Padmakumar & He, 2024; Seddik et al., 2024; Dohmatob et al., 2024) when training on self-generated outputs, by only slightly denoising the dataset each time and by performing corruption-aware diffusion training (e.g. as in Ambient Diffusion (Daras et al., 2025c,b, 2023)). The latter is used to account for errors that happen during the denoising process of the previous round and avoid propagating these errors to the next iteration. Experimentally, Ambient Dataloops consistently outperforms prior work on learning from corrupted data in both controlled settings, as well as in real datasets, including text-conditional models trained on dozens of millions of samples and generative models for protein structures. We

further provide theoretical justification for the potential effectiveness of the approach in settings where the initial score estimation is sufficiently accurate.

2 Background and Related Work

Diffusion Models. Diffusion modeling (Sohl-Dickstein et al., 2015; Ho et al., 2020; Song & Ermon, 2019; Song et al., 2021) is one of the most prominent frameworks for learning high-dimensional, complex, continuous distributions. The main algorithmic idea is to consider not only the target density, which we will denote with p_0 , but a family of intermediate distributions, $p_t = p_0 \circledast \mathcal{N}(0, \sigma(t)^2 I)$, where $\sigma(t)$ is an increasing function and t is a continuous variable in $[0, T]$ (for some big constant T) representing the diffusion time. We denote with X_0 the R.V. sampled according to the target density p_0 and similarly $X_t = X_0 + \sigma(t)Z$, $Z \sim \mathcal{N}(0, \sigma(t)^2 I)$ the R.V. sampled according to p_t . During training, the object of interest is the best l_2 denoiser for each one of these intermediate densities, i.e. the conditional expectation of the clean sample given a noisy observation, $\mathbb{E}[X_0 | X_t = \cdot]$. The latter is typically optimized with the following objective:

$$J(\theta) = \mathbb{E}_{t \in \mathcal{U}[0, T]} \mathbb{E}_{X_0} \mathbb{E}_{X_t | X_0, t} \left[\|h_\theta(X_t, t) - X_0\|^2 \right]. \quad (1)$$

For a sufficiently rich parametrization family, the minimizer of this objective is indeed the conditional expectation, i.e. $h_{\theta^*}(\cdot, t) = \mathbb{E}[X_0 | X_t = \cdot]$. The latter is connected to the score-function $\nabla \log p_t(\cdot)$ through Tweedie’s formula (Tweedie, 1957; Efron, 2011) and it can be used to sample according to a diffusion process (Song et al., 2021; Anderson, 1982).

Finite datasets and imperfect data. In practice, we don’t have access to infinite samples from p_0 but to a finite number, denote n_1 . When n_1 is small, diffusion models often memorize their training set and learn the empirical distribution \hat{p}_0 (Shah et al., 2025; Daras et al., 2024; Somepalli et al., 2023a,b; Carlini et al., 2023; Kamb & Ganguli, 2025; Kadkhodaie et al., 2024).

One way to increase the sample size and improve generalization is to incorporate low-quality or out-of-distribution data that is usually cheaper and more widely available. This occurs naturally in many datasets or can be collected (e.g. data scraping, synthetic data from other models, etc). To avoid hurting the generation quality or biasing the distribution, it is crucial to account for the corruption of this additional data during the training of the diffusion model. Over the past few years, there have been numerous proposed methods for training generative models with imperfect data (Bora et al., 2018; Daras et al., 2023, 2024, 2025a,c,b; Aali et al., 2023, 2025; Lu et al., 2025; Kelkar et al., 2024; Rozet et al., 2024; Bai et al., 2025; Zhang et al., 2025; Tewari et al., 2023; Liu et al., 2025; Alemdohmeh et al., 2024b). The majority of these works make some assumption about the nature of the degradation in the given data, which is limiting if we want to apply these datasets to Web-scale real datasets that have samples of various qualities and unknown corruption types.

Daras et al. (2025b,c) propose an approach for dealing with data of various qualities without an explicit degradation model. The central idea is that the distance between any two distributions, p_0 and q_0 , contracts with the introduction of noise. In this work, q_0 is the distribution obtained by sampling from p_0 but via an unknown noisy measurement process. For a sufficiently high amount of noise, t_n , the distributions p_{t_n} and q_{t_n} approximate well each other. Hence, for noise levels $t \geq t_n$, we can use samples from a low-quality or out-of-distribution data-source q_0 to increase the pool size of available data for a small distribution bias penalty. Daras et al. (2025c) analyze this bias-variance trade-off and provide rigorous ways for deciding the threshold t_n beyond which it is beneficial to incorporate q_0 data. After annotation, each sample from $Y_0 \sim q_0$ is mapped to its noisy version Y_{t_n} and the problem amounts to training a diffusion with a mixture of clean data (from p_0) and samples corrupted with additive Gaussian noise (that are well approximated as coming from p_{t_n}). For details see Appendix Section E.

The reduction of the problem to the additive noise case enables the leveraging of well-developed statistical tools for learning from noisy data (Stein, 1981; Lehtinen et al., 2018; Moran et al., 2020; Daras et al., 2024, 2025a). In particular, it is possible to learn the conditional expectation of the clean samples with noisy targets. In the most general form, we are given access to a dataset \mathcal{D} where each sample has a known noise level t_i and can be used for diffusion times in $[t_i, T]$. The two extremes are $t_i = 0$ (clean sample, used everywhere) and $t_i = T$ (filtering, the sample is not used at all). Daras et al. (2024) establish that for $\alpha(t, t_i) = \frac{\sigma^2(t) - \sigma^2(t_i)}{\sigma^2(t)}$, given enough data, the following

objective has the same minimizer as equation 1, but it does so without having access to clean targets:

$$J_{\text{ambient-}o}(\theta) = \mathbb{E}_{t \in \mathcal{U}[0, T]} \sum_{i: t_i < t} \mathbb{E}_{x_t | x_{t_i}} \left[\|\alpha(t, t_i)h_\theta(x_t, t) + (1 - \alpha(t, t_i))x_t - x_{t_i}\|^2 \right], \quad (2)$$

3 Method

Problem Setting. We study exactly the same problem as Daras et al. (2025c,b,a, 2024); in particular, we assume that we have access to a dataset of samples $\mathcal{D}_0 = \{(x_{t_i}, t_i)\}_{i=1}^N$ where each sample x_{t_i} is (at least approximated as) being sampled from a density p_{t_i} . As explained in Section 2, this dataset is typically formed by starting with a dataset that contains some clean samples and some samples of unknown types and then adding the appropriate amount of noise to the corrupted samples to make them look approximately as clean samples corrupted with additive noise. In Section 5, we experiment with such transformed datasets. For the simplicity of the presentation, we avoid detailing this procedure in the main text, but we provide all the necessary information in Appendix Section E. We also refer the interested reader to (Daras et al., 2025c) for more details about how this initial reduction from arbitrary degradations to the additive Gaussian noise case can be performed.

Algorithm. Our method is summarized in Figure 2. It iterates between two steps, for $l = 1, \dots$:

- ◊ **Model Training.** At this step, we take the training set $\mathcal{D}^{(l-1)}$ and then we train a new model on this dataset. Since the dataset has noisy data, we use the training objective of Equation 2. This is the standard step performed in prior work, e.g., see (Daras et al., 2025c,b,a, 2024).
- ◊ **Dataset Restoration.** At the end of the model training, we have a model $h_{\theta^{(l)}}$. Our method uses this network to *denoise* the *original dataset*. In particular, we perform posterior sampling $X_{t_i/2^l} \sim p_{\theta^{(l)}, t_i/2^l}(\cdot | x_{t_i}, t_i)$ and add $(X_{t_i/2^l}, t_i/2^l)$ to a new dataset $\mathcal{D}^{(l)}$. Simply put, this procedure synthetically reduces the noise level of the original dataset by denoising from t to $t/2^l$ using the best prior model available at iteration l . The constant 2 effectively controls the amount of progress we expect each iteration of this algorithm to achieve, and in practice, it can be tuned as a hyperparameter.

A complete description of the algorithm is provided in Algorithm 1.

Discussion. The crux of this algorithm is dataset refinement; at each loop, we use the best model we have to improve the dataset by reducing the amount of noise in its samples. The resulting dataset can be used for a new training and so forth. As we run more loops, the model becomes better, and hence we take bigger denoising steps. We provide an overview of the approach in Figure 2.

Comparison with Ambient Diffusion Omni. In (Daras et al., 2025c), the low-quality parts of the dataset are getting noised to a particular diffusion time, and they can only be used during training for times that correspond to higher noise than the noise level they got mapped to. This is the starting point of our method (loop 0). However, after a successful training, we can now use the model to partially denoise these original noisy points and perform a new training on the resultant dataset.

Potential limitations. The idea of dataset refinement, despite being natural, has three issues. First, it seems to be violating the data processing inequality; information cannot be created out of thin air, and hence any processing of the original data cannot have more information for the underlying distribution than the original dataset. While this is true, it is important to consider that the first training might be suboptimal due to failures of the optimization process (e.g., gradient descent getting stuck in a local minimum). Hence, dataset refinement can be thought of as a reorganization of the original information in a way that facilitates learning and creates a better optimization landscape.

Another challenge for our method is that we train on synthetic data. Several recent works have shown that naive training on synthetic data leads to catastrophic self-confusing loops and mode collapse (Alemohammad et al., 2024a; Shumailov et al., 2024; Hataya et al., 2023; Martínez et al., 2023; Padmakumar & He, 2024; Seddik et al., 2024; Dohmatob et al., 2024). Our key idea to get around this issue is to treat the restorations as *noisy* data as well, just at a smaller noise level compared to where the restoration started. In particular, we do not run the full posterior sampling algorithm; we early stop the generation process at time $t_i/2^l$ at each round l . Prior work has shown that the catastrophic self-consuming loops can be avoided using a *verifier* that assesses the quality of the generations (Ferbach et al., 2024; Feng et al., 2024; Zhang et al., 2024). The gradual denoising

Algorithm 1 Ambient Dataloops Training Algorithm.

Require: dataset $\mathcal{D}^{(0)} = \{(x_{t_i}, t_i)\}_{i=1}^N$, noise scheduling $\sigma(t)$, batch size B , diffusion time T , number of loops L , random weights $\theta^{(0)}$.

- 1: **for** $l \in [1, L]$ **do** ▷ A new loop starts.
- 2: $\theta^{(l)} \leftarrow \theta^{(l-1)}$ ▷ Initialize from the weights of the previous round (finetuning).
- 3: **while** not converged **do** ▷ A new training starts.
- 4: $t_{s_1}, \dots, t_{s_B} \leftarrow$ Sample uniformly B times in $[0, T]$
- 5: $(x_{\bar{t}_1}, \bar{t}_1), \dots, (x_{\bar{t}_B}, \bar{t}_B) \leftarrow$ Sample (at random) points from $\mathcal{D}^{(l-1)}$ that can be used for times t_{s_1}, \dots, t_{s_B} , i.e. points that have lower noise level than the corresponding t_{s_i} .
- 6: $\text{loss} \leftarrow 0$ ▷ Initialize loss.
- 7: **for** $(x_{\bar{t}_i}, \bar{t}_i, t_{s_i}) \in (x_{\bar{t}_1}, \bar{t}_1, t_{s_1}), \dots, (x_{\bar{t}_B}, \bar{t}_B, t_{s_B})$ **do**
- 8: $\epsilon \sim \mathcal{N}(0, I)$ ▷ Sample noise.
- 9: $x_{t_{s_i}} \leftarrow x_{\bar{t}_i} + \sqrt{\sigma^2(t_{s_i}) - \sigma^2(\bar{t}_i)}\epsilon$ ▷ Add additional noise.
- 10: $\alpha(t_{s_i}, \bar{t}_i) \leftarrow \frac{\sigma^2(t_{s_i}) - \sigma^2(\bar{t}_i)}{\sigma^2(t_{s_i})}$,
- 11: $w(t_{s_i}, \bar{t}_i) \leftarrow \frac{\sigma^4(t_{s_i})}{(\sigma^2(t_{s_i}) - \sigma^2(\bar{t}_i))^2}$. ▷ Loss reweighting.
- 12: $\text{loss} \leftarrow \text{loss} + w(t_{s_i}, \bar{t}_i) \|\alpha(t_{s_i}, \bar{t}_i)h_{\theta^{(l)}}(x_{t_{s_i}}, t_{s_i}) + (1 - \alpha(t_{s_i}, \bar{t}_i))x_{t_{s_i}} - x_{\bar{t}_i}\|^2$
- 13: **end for**
- 14: $\text{loss} \leftarrow \frac{\text{loss}}{B}$ ▷ Compute average loss.
- 15: $\theta^{(l)} \leftarrow \theta^{(l)} - \eta \nabla_{\theta^{(l)}} \text{loss}$ ▷ Update network parameters via backpropagation.
- 16: **end while**
- 17: $\mathcal{D}^{(l)} = \emptyset$
- 18: **for** $(x_{t_i}, t_i) \in \mathcal{D}^{(0)}$ **do** ▷ A new restoration cycle starts.
- 19: $x_{t_i/2^l} \sim p_{\theta^{(l)}, t_i/2^l}(\cdot | x_{t_i}, t_i)$ ▷ Perform posterior sampling from t_i to $t_i/2^l$.
- 20: $\mathcal{D}^{(l)} \leftarrow \mathcal{D}^{(l)} \cup (x_{t_i/2^l}, t_i/2^l)$ ▷ Add restored point to dataset.
- 21: **end for**
- 22: **end for**

and the finite number of rounds in our algorithm have a similar effect. Tuning the number of rounds wisely prevents the model from attempting to denoise the dataset at a level beyond what's possible using the available training set. Naturally, tuning this parameter in practice is not straightforward, and we provide ablations of miscalibration in our experiments.

The last issue associated with our approach has to do with the associated computational requirements. At each round, we have to restore the whole dataset and then fine-tune the model, leading to an increase in the training cost. Indeed, our method is useful when data, not compute, is the bottleneck. If there is more data available, it is always better to use it as fresh samples reveal more about the underlying distribution (Goyal et al., 2024) and there is no need to perform the expensive restoration step that our method requires. However, if there is lack of data, our framework is useful as it attempts to extract as much utility as possible from the given training set.

4 Theoretical Modeling

In this section, we study the theoretical aspects of the proposed method. We consider a stylized setting and version of the algorithm, arguing that if the score function is sufficiently well-approximated after the first iteration, then performing a *dataset refinement* step can improve the estimation error.

Setting. For the purposes of the theoretical analysis, we adopt the theoretical setting from Ambient Omni (Daras et al., 2025c), and identify conditions under which *dataset looping* is beneficial.

In the description of our method, we assumed that we have access to a dataset $\mathcal{D}_0 = \{(x_{t_i}, t_i)\}_{i=1}^N$, where each datapoint comes with a threshold time t_i indicating that we will use it to estimate scores for diffusion times $t \geq t_i$. As discussed earlier, the way those samples and associated threshold times came about is as follows: Some are samples from the target distribution p_0 , and all these samples are assigned a threshold time 0. Then there are samples from distributions different from p_0 . If some sample was sampled from some distribution q_0 , we would add to it noise sampled from $\mathcal{N}(0, \sigma_{t_i}^2 I)$ and assign to the resulting noised sample threshold time t_i , where the choice of t_i depends on the

distance between p_0 and q_0 . The choice would be such that p_{t_i} and q_{t_i} are sufficiently close that for $t \geq t_i$ we prefer to include this sample in estimating scores versus not using it. Choosing those times correctly is complex, but the theoretical analysis in Ambient Omni provides us guidance for how to choose these times, in the case where all samples either come from p_0 or from q_0 , as described below. So let us stick to this case for our analysis here as well.

In particular, we are given n_1 samples from a target distribution p_0 that we want to learn to generate. We assume that p_0 is supported on $[0, 1]$ and is λ_1 -Lipschitz. We are also given n_2 samples from a distribution q_0 , which is not the target distribution, and may have some distance from p_0 . We assume that q_0 is λ_2 -Lipschitz. We want to train a diffusion model to sample p_0 , so we need to learn the score functions of all distributions $p_t = p_0 \circledast \mathcal{N}(0, \sigma_t^2 I)$. Given our n_1 i.i.d. samples from p_0 we can create n_1 i.i.d. samples from p_t . Given our n_2 i.i.d. samples from q_0 we can also create n_2 i.i.d. samples from $q_t = q_0 \circledast \mathcal{N}(0, \sigma_t^2 I)$, but again q_t is different from p_t . The observation that Daras et al. (2025c) leverage is that q_t is closer to p_t than q_0 is to p_0 because convolution with a Gaussian distribution contracts distances.

Because of this contraction, it could be that for sufficiently large t 's (a.k.a. σ_t 's), we are better off including the n_2 (biased) samples from q_t to estimate p_t rather than only using the unbiased samples from p_t . Indeed this is what is shown by Daras et al. (2025c) in Ambient Omni, as discussed below.

Prior results. For any diffusion time t , Daras et al. (2025c) compare the accuracy attained by the following algorithms:

- **Algorithm A:** Use the n_1 samples from p_t and estimate p_t using denoising diffusion training.
- **Algorithm B:** Use $(n_1 + n_2)$ samples from the mixture density $\tilde{p}_t = \frac{n_1}{n_1 + n_2} p_t + \frac{n_2}{n_1 + n_2} q_t$ and estimate p_t using denoising diffusion training by pretending that all training samples are from p_t .

Using a connection between diffusion training and kernel density estimation, Daras et al. (2025c) propose a criterion for when to use Algorithm B over Algorithm A. Specifically, they show that, with probability $1 - \delta$ over the randomness in the samples, the error in total variation distance between the density estimated by Algorithm B and p_t can be upper bounded by:

$$\begin{aligned} \text{Error using } n_1 + n_2 \text{ samples from } \tilde{p}_t &\lesssim \frac{1}{(n_1 + n_2)} + \frac{1}{\sigma_t^2(n_1 + n_2)} + d_{\text{TV}}(p_t, \tilde{p}_t) \\ &+ \sqrt{\frac{\log(n_1 + n_2) + \log(1 \vee \frac{n_1}{n_1 + n_2} \lambda_1 + \frac{n_2}{n_1 + n_2} \lambda_2) + \log 2/\delta}{\sigma_t^2(n_1 + n_2)}}, \end{aligned} \quad (3)$$

while the error made by Algorithm A can be upper bounded by:

$$\text{Error using } n_1 \text{ samples from } p_t \lesssim \frac{1}{n_1} + \frac{1}{\sigma_t^2 n_1} + \sqrt{\frac{\log n_1 + \log(1 \vee \lambda_1) + \log 2/\delta}{\sigma_t^2 n_1}}, \quad (4)$$

where \lesssim hides absolute constants in both cases. Thus, Daras et al. (2025c) propose a concrete criterion for when to choose Algorithm B over Algorithm A, namely for times t such that:

$$\text{RHS of equation 3} \leq \text{RHS of equation 4}. \quad (5)$$

For the purposes of applying the criterion, they also show that:

$$d_{\text{TV}}(p_t, \tilde{p}_t) \lesssim \frac{n_2}{\sigma_t(n_1 + n_2)} d_{\text{TV}}(p_0, q_0).$$

Improved results through looping. The theory of Ambient Omni compared (1) using only samples from the true distribution p_t (Algorithm A), or (2) using samples from \tilde{p}_t which is a mixture of the true distribution p_t and the biased distribution q_t (Algorithm B). However, there are more options. Our datalooping algorithm motivates the following alternate algorithm:

- **Algorithm C:** Transform samples from q_t using a (potentially stochastic and learned) mapping function f . This defines the push-forward measure $\bar{q}_t = f \# q_t$. Then, learn using $(n_1 + n_2)$ samples from the distribution: $\tilde{p}_t = \frac{n_1}{n_1 + n_2} p_t + \frac{n_2}{n_1 + n_2} \bar{q}_t$.

Notice that Algorithm C is a generalization of Algorithm B, as the latter is recovered using the identity transformation function. Denote by $p_{t, \text{approx}}^{(L)}$ the approximate density estimated by Algorithm L, for $L \in \{A, B, C\}$. It is straightforward to show the following lemma:

Lemma 1 (Contractive transformations lead to better learning). *If the mapping function f contracts the TV distance with respect to the underlying true density p_t , i.e., if for any density ϕ it holds that:*

$$d_{\text{TV}}(f\#\phi, p_t) \leq d_{\text{TV}}(\phi, p_t), \quad (6)$$

then, in all cases where Algorithm B is preferable to Algorithm A, according to Criterion 5, Algorithm C is weakly preferable to Algorithm B, and it is strictly preferable if equation 6 is strict.

The lemma's statement is intuitive; if we have a way to “correct” the samples from the out-of-distribution density q_t , we should be able to achieve a better approximation to p_t if we were to correct them versus using them as is. See appendix 1 for the full proof. A related work (Gillman et al., 2024) studies the implications of having an idealized corrector function for learning from bad data (in their case, synthetic data) and establishes asymptotic convergence to the underlying distribution. Our result is similar in spirit, but the analysis is based on the bounds established by thinking about the implicit kernel-density estimation that diffusion modeling obtains.

With the above observations in place, let us identify conditions under which an idealized variant of Algorithm 1 would reduce the estimation error after one iteration of dataset refinement. In particular, suppose that all the correct scores were known and we perform posterior sampling of X_t given $X_{t'}$ for all $X_{t'} \sim q_{t'}$ and some $t' > t$. This would correspond to running the reverse diffusion process (Anderson, 1982; Oksendal, 2013) initializing at $X_{t'} \sim q_{t'}$ from time t' down to time t :

$$dX_\tau = -\nabla \log p_\tau(X_\tau) d\tau + \sqrt{2} d\bar{B}_\tau, \quad (7)$$

where \bar{B}_t is a reverse time Brownian motion (that is 0 at time t'). Suppose that $f_{t',t}$ is the randomized map that takes a sample from q_t adds Gaussian noise to it to produce a sample $X_{t'} \sim q_{t'}$, then runs the backwards diffusion equation 7 from t' down to t . We show that under appropriate assumptions, the sampled distribution $f_{t',t}\#q_t$ is closer to p_t compared to q_t . Thus, Algorithm C, using samples from $f_{t',t}\#q_t$ would have better estimation error compared to Algorithm B using samples from q_t per Lemma 1.¹ This theory applies to any number of loops as long as the diffusion model can sample from p_t . We show the following for general dimensional measures. To state the theorem, suppose that ρ_t is the measure of X_t when we run the backwards diffusion process starting at $t' > t$, initializing $X_{t'} \sim q_{t'}$:

Lemma 2 (Non-Expansion and Contraction under Log-Sobolev). *For $f_{t',t}$ as defined above, it holds, for any f -divergence, that:*

$$D_f(f_{t',t}\#q_t, p_t) \leq D_f(q_t, p_t),$$

Moreover, if i. p_0 is supported in $B(0, R)$ and t is large enough or p_0 satisfies a log-Sobolev inequality with constant C , ii. $\|\frac{\rho_\tau}{p_\tau}\|_\infty \in [1/B, B]$ for some $B > 0$ and all $\tau \in [t, t']$, and iii. $\|\frac{\partial}{\partial \tau} \log p_\tau\|_{L^2(p_\tau)} < A$ for all $\tau \in [t, t']$, then:

$$D_{\text{KL}}(f_{t',t}\#q_t, p_t) \leq (1 - C') D_{\text{KL}}(q_t, p_t),$$

for some $C' < 1$ that depends on A, B and C or R (whichever is applicable) but not the dimension, unless $D_{\text{KL}}(f_{t',t}\#q_t, p_t)$ drops below another absolute constant that depends on A, B and C or R (whichever is applicable) but not the dimension. See appendix 2 for the proof.

Learning Errors. The above describes what the framework would achieve in an idealized scenario where we have access to the true scores. The issue is that in practice, we cannot run Eq. 7 since we only have an approximation to the true score. To wit, our looping framework *approximates* the score function with the *best estimator using the current data*. In particular, for times t for which Algorithm B is preferred to Algorithm A, the estimation we have from the first round is:

$$\nabla \log p_{t,\text{approx}}^{(2)}(x) = \frac{1}{(n_1 + n_2) \sqrt{2\pi\sigma_t^2}} \left(\sum_{i=1}^{n_1} w(x, x_i)(x - x_i) + \sum_{i=1}^{n_2} w(x, x'_i)(x - x_i) \right), \quad (8)$$

where $w(x, y) = \mathcal{N}(x; \mu = y, \sigma = \sigma_t^2)$, and $\{x_i\}_i$ are the samples from p_t while $\{x'_i\}_i$ are the samples from q_t . This score only approximates the desired one, $\nabla \log p_t$. Due to this estimation error, running the Langevin Diffusion process of Eq. 7 would perform worse in terms of contraction towards $p_{t'}$. In practice, our experiments show that our estimates are sufficiently good estimates of the score function, and hence Algorithm C obtains faster rates of convergence than Algorithms A or B.

¹Formally, to combine the second part of Lemma 2 with Lemma 1, one needs an adaption of the latter for KL.

Table 1: Unconditional and conditional results for CIFAR-10 with 90% corrupted and 10% clean data.

Corruption	Filtering	No Filtering	Ambient Omni (Loop 0)	Ambient DataLoops (Loop 1)	FID (\downarrow)	σ_{\min}	LPIPS (\downarrow)	MSE (\downarrow)	C-FID (\downarrow)	LPIPS (\downarrow)	MSE (\downarrow)	C-FID (\downarrow)
	$\sigma_B = 0.6$	$\sigma_B = 0.8$	$\sigma_B = 1.0$	$\sigma_B = 50$			$\sigma_B = 25$	$\sigma_B = 18$				
Blur	$\sigma_B = 0.6$	8.79	11.26	$\sigma = 1.2$	5.689 ± 0.0209	$\rho = 1.2/2^3$	4.947 ± 0.0572					
	$\sigma_B = 0.8$	8.79	28.26	$\sigma = 1.9$	5.938 ± 0.0583	$\rho = 1.9/2^3$	5.044 ± 0.0709					
JPEG	$\sigma_B = 1.0$	8.79	45.32	$\sigma = 2.4$	6.080 ± 0.0758	$\rho = 2.4/2^3$	5.358 ± 0.0644					
	$q = 50$	8.79	61.67	$\sigma = 1.2$	5.836 ± 0.0674	$\rho = 1.2/2^3$	4.825 ± 0.0665					
	$q = 25$	8.79	91.55	$\sigma = 1.3$	6.188 ± 0.0456	$\rho = 1.3/2^3$	5.531 ± 0.0742					
	$q = 18$	8.79	112.43	$\sigma = 1.6$	6.261 ± 0.0624	$\rho = 1.6/2^3$	5.464 ± 0.0586					

(a) Unconditional metrics

(b) Conditional metrics

5 Experimental Results

5.1 Controlled experiments with known corruptions

Experimental Setting. We start our experiments by validating our approach in controlled settings. We follow the experimental methodology of the Ambient Omni paper; in particular, we train models on CIFAR-10 by corrupting 90% of the dataset with Gaussian Blur and JPEG compression at various degradation levels while keeping 10% of the dataset intact. We use the parameter σ_B to refer to the standard deviation of the Gaussian kernel used for blurring the dataset images and the parameter q to denote the file size after JPEG compression compared to the original file size.

We compare with the following baselines: **a)** quality-filtering (training only on the clean data), **b)** treating all-data as equal, and, **c)** Ambient Omni (Daras et al., 2025c), which is currently the state-of-the-art for learning diffusion generative models from corrupted data with unknown degradation types. We always initialize our method with the Ambient Omni checkpoints (loop 0). We further directly take the mapping between the low-quality samples (e.g. blurry/JPEG images) and their corresponding noising time (see Section 2 and E) from the work of Daras et al. (2025c), when needed. For all the experiments in this paper, we provide full details in Appendix Section D.

Unconditional and Conditional Metrics. We present unconditional FID results for all the baselines and one loop of our method in Table 1 (top). As shown, even a single loop of our proposed method leads to consistent and significant FID improvements up to 17% reduction in FID. We emphasize that for all of the reported results, we always train the underlying models until performance saturates, and we report from the available checkpoints the one that achieves the best FID. This is to ensure that our method (which requires additional compute) does not have an unfair advantage. In the experimental settings we study, we are limited by the availability of data, not compute.

One benefit of starting our experimental analysis on this controlled setting is that we have the ground truth for the corrupted samples, and hence we can report conditional metrics too. We report conditional FID, LPIPS and MSE. Conditional FID is defined as follows; for each sample (x_{t_i}, t_i) in the dataset we use a given model h_θ to sample from $\bar{X}_0 \sim p_{\theta,0}(\cdot | x_{t_i}, t_i)$, where $p_{\theta,0}(\cdot | x_{t_i}, t_i)$ is the distribution that arises by running the learned reverse process initialized at time $t = t_i$ with the noisy sample x_{t_i} . We then compute the FID between the set sampled with posterior sampling and the reference set. MSE and LPIPS are point-wise restoration metrics and hence it is more meaningful to compute them by measuring the distance of the ground-truth sample to the posterior mean, rather than any random sample from the posterior distribution. In particular, for each sample (x_{t_i}, t_i) in the dataset we use a given model h_θ to estimate with Monte Carlo the posterior mean defined as $\mathbb{E}_{\bar{X}_0 \sim p_{\theta,0}(\cdot | x_{t_i}, t_i)}[\bar{X}_0]$. For a perfectly trained model and ignoring discretization errors, this quantity equals $h_\theta(x_{t_i}, t_i)$, but we use the former quantity to account for learning and sampling errors. We report our conditional results in Table 1 (bottom). Interestingly, although unconditional FID is always better for the model after the loop, this is not always the case for the conditional metrics. A corollary is that if we use the L1 model to restore the dataset, we might yield worse performance compared to stopping after 1 loop. This can happen, as seen below.

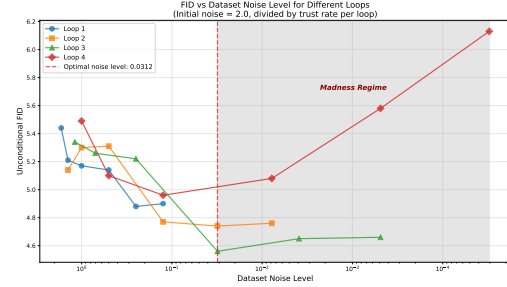


Figure 3: Multiple loops and ablation on the rate of progress. The horizontal axis is the noise level we denoise a corrupted CIFAR-10 dataset after k loops, where k changes for each one of the lines. Going too fast or too slow is suboptimal. There is a point after which reducing the dataset further only hurts (madness regime) because the current model has reached its denoising capacity. FID is always computed wrt to the original clean CIFAR-10.

Multiple loops and rate of progress. Roughly speaking, there are two reasons that can lead to deterioration in performance. The first has to do with the inherent limit on how much a finite dataset can be denoised reliably. Attempting to go beyond this limit will cause any algorithm to fail. The second reason has to do with the optimization (looping) process, i.e. with *how we reach the denoising limit*. We investigate this extensively in Figure 3 and Table 3. The figure shows the effect of bringing the dataset to a noise level by running one or more loops. Going too fast or too slow is hurtful, due to overconfidence in the model’s capabilities or accumulation of errors, respectively. Further, there is a limit to how much we can safely denoise the dataset, after which limit we reach the “madness regime” (Alemohammad et al., 2024a) where performance degrades significantly. The optimal performance for the blurring corruption with $\sigma_B = 0.6$ is achieved with 3 loops, where the dataset noise level is reduced by 8 each time. On the other hand, if we cannot afford running multiple loops, Table 3 suggests that taking a larger denoising step for one loop is preferable.

Other ablations. Beyond the number of loops and the rate of denoising progress, we provide numerous ablations in the Appendix that quantify the role of different aspects of our approach. In particular, Figure 5 shows that the improvements are across all diffusion times, Table 5 shows that there are benefits in sampling multiple times from the posterior, and 4 shows the effect of restoring the dataset of the previous round compared to always restoring the original dataset. The main takeaway is that by carefully tuning parts of the pipeline, we can further boost performance. For example, in the Appendix, we manage to push the unconditional FID for $\sigma_B = 0.6$ on CIFAR from the 5.34 reported in Omni all the way to 4.52. While such improvements are possible, we run the majority of the experiments in the main paper with the simplest variant of our method, as it achieves comparable performance and is far more educational to the reader.

5.2 Experiments with synthetic data and text-to-image models

Having established the effectiveness of the method in controlled settings, we are now ready to test our algorithm in real use cases. In particular, we experiment with text-to-image generative modeling, following the architectural and dataset choices of MicroDiffusion (Sehwag et al., 2025). Sehwag et al. (2025) train a diffusion model from scratch using only 8 GPUs in 2 days. During that training, 4 datasets are used; Conceptual Captions (12M) (Sharma et al., 2018), Segment Anything (11M) (Kirillov et al., 2023), JourneyDB (4.2M) (Sun et al., 2023), and DiffusionDB (10.7M) (Wang et al., 2022). Daras et al. (2025c) noticed that DiffusionDB, despite contributing 28.23% of the dataset samples, contains synthetic images that have significantly lower quality than the rest of the dataset. To account for this, the authors noise the DiffusionDB dataset to level $\sigma_{\text{DiffusionDB}} = 2.0$ and only use it to train for diffusion times $t : \sigma_t \geq 2.0$. This leads to a significant COCO FID improvement compared to using it as clean; FID drops from 12.37 to 10.61.

We now attempt to further improve the performance by taking the model trained by Daras et al. (2025c) to denoise the DiffDB dataset and then train a new model on the denoised set. Consistent with the description of our algorithm in Section 3, we do partial dataset restoration by performing posterior sampling to bring the DiffDB dataset at noise level $\sigma'_{\text{DiffusionDB}} = \sigma_{\text{DiffusionDB}}/2 = 1.0$. We then train the model on this denoised dataset, using the Ambient Diffusion training objective equation 2, as usual. The resulting model achieves further improvements to COCO FID and CLIP-FD score, as shown in Table 2 and scores comparable at GenEval (GPT-4o evaluations) across different categories. Figure 1 shows examples of images from DiffDB and their evolution across our looping process. As seen, the datasets seem to be converging after 1 loop.

Table 2: Quantitative benefits of Ambient Loops on COCO zero-shot generation and GenEval.

Method	COCO (Fidelity & Alignment)		GenEval Benchmark						
	FID-30K (↓)	Clip-FD-30K (↓)	Overall	Single	Two	Counting	Colors	Position	Color attribution
Micro-diffusion	12.37	10.07	0.44	0.97	0.33	0.35	0.82	0.06	0.14
Ambient-o (L0)	10.61	9.40	0.47	0.97	0.40	0.36	0.82	0.11	0.14
Ambient Loops (L1)	10.06	8.83	0.47	0.97	0.38	0.35	0.78	0.11	0.19

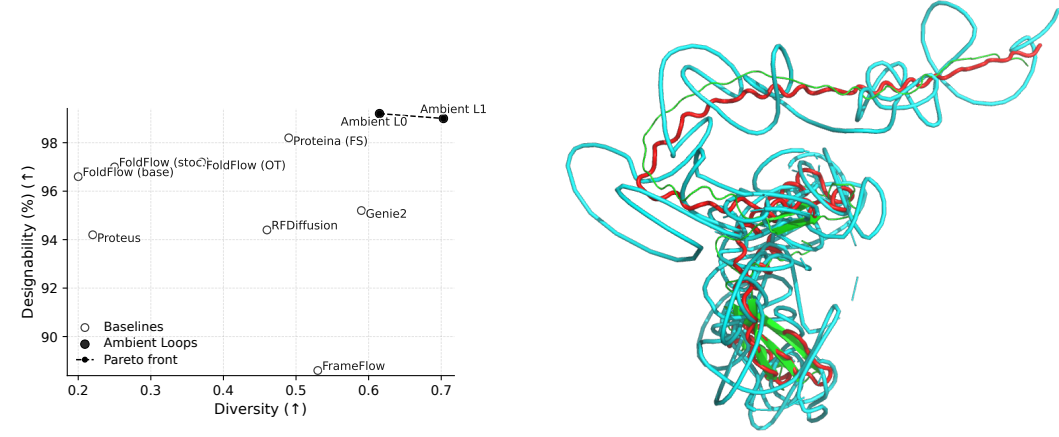
5.3 De-novo protein design

Introduction. For this final part of our experimental evaluation, we switch modality and target structural protein design. This problem is significant because accurate de novo protein structure models can result in improved designs for new vaccines, therapeutics, and enzymes. The problem is

also well-suited for our Ambient Dataloops framework, as techniques for determining the atomistic resolution of molecular protein structures (such as X-ray crystallography) are inherently noisy. On top of that, acquiring samples through such techniques requires domain expertise and significant resources and hence the available datasets, such as the Protein Data Bank, are of limited size. To enrich the dataset, recent state-of-the-art models for protein backbones are trained on synthetic data from AlphaFold, which once again contain corrupted samples due to learning errors in folding.

Setting. Daras et al. (2025b) applied the Ambient Omni (Daras et al., 2025c) framework to train a generative model for protein backbones. We use the same dataset, architectural, and training procedures as in (Daras et al., 2025b) to demonstrate that looping can improve performance in domains beyond Computer Vision. In particular, we start with the dataset of Daras et al. (2025b) that contains 90,250 structurally unique proteins from the AlphaFold Data Bank (AFDB) dataset, with a maximum length of 256 residues. To find the associated noise level of the dataset we follow once again the experimental protocol of the authors, which is to map proteins to diffusion times according to AlphaFold’s self-reported confidence for the predicted structure as given by the pLDDT score. We then use the Ambient Proteins (Daras et al., 2025b) model to denoise its training set and we start a new training run on the denoised dataset. One example of such a denoising is given in Figure 4b. In agreement with the rest of the paper, we also treat the denoised dataset as noisy, but at a lower noise level. In this particular domain, we use the existing pLDDT to diffusion time mapping from Ambient Proteins (Daras et al., 2025b) and we treat the denoised predictions as increasing the pLDDT (synthetically) by 3 points in each denoised sample. We arrived at this value after ablating different pLDDT adjustments that led to inferior results. To assess the quality of the trained models, we use the two most established metrics in the field: Designability and Diversity. There is a trade-off between the two metrics that defines a Pareto frontier in the joint space.

Results. Just one loop of our procedure is enough to achieve a new Pareto point, as shown in Figure 4a. In particular, we trade 0.2% decrease in designability for a 14.3% increase in diversity, significantly expanding the creativity boundaries of the loop 0 model for the same inference parameters. Both models dominate in the Pareto frontier over other baselines showing both the promise of degradation-aware diffusion training and the potential of datalooping to enhance the generative capabilities for protein design. While our protein evaluation is preliminary and the results need to be verified in the wet lab, the metrics suggest that datalooping could be useful for scientific domains.



(a) Designability-Diversity trade-off for de novo design of protein backbones. Training with Ambient Proteins dominates the Pareto frontier. One loop of our framework achieves a 14.3% increase in diversity for a minor 0.2% in designability.

(b) Example of our dataset refinement procedure. An initial low pLDDT protein, denoted with green, is noised to a certain level, giving the shape in cyan. We initialize the reverse process with the cyan sample, and we sample the red point from the posterior.

Figure 4: (a) Pareto frontier for protein backbone design. (b) Example point refinement procedure.

6 Conclusions and Future Work

We introduced Ambient Dataloops, a framework that enables better learning of the underlying data distribution by refining the dataset together with the model being trained. This algorithm paves the way for denoising scientific datasets where sample quality naturally varies and it has the potential to improve not only generative models but also supervised models optimized for downstream applications.

7 Reproducibility statement

We detail proofs for the lemmas used in the main text in Appendix Section A. We detail training hyper-parameters, computational requirements, and the evaluation pipeline in Appendix Section D. We additionally make all our training code available in the following repository.

8 Acknowledgements

Experiments conducted in the UT Austin Vista cluster. Adrian Rodriguez-Munoz is supported by a DSTA, Singapore grant.

References

Asad Aali, Marius Arvinte, Sidharth Kumar, and Jonathan I. Tamir. Solving inverse problems with score-based generative priors learned from noisy data. In *2023 57th Asilomar Conference on Signals, Systems, and Computers*, pp. 837–843. IEEE, October 2023. doi: 10.1109/ieeeconf59524.2023.10477042. URL <http://dx.doi.org/10.1109/IEEECONF59524.2023.10477042>.

Asad Aali, Giannis Daras, Brett Levac, Sidharth Kumar, Alex Dimakis, and Jon Tamir. Ambient diffusion posterior sampling: Solving inverse problems with diffusion models trained on corrupted data. In *The Thirteenth International Conference on Learning Representations*, 2025. URL <https://openreview.net/forum?id=qeXcMutEZY>.

Tara Akhoud-Sadegh, Jarrid Rector-Brooks, Avishek Joey Bose, Sarthak Mittal, Pablo Lemos, Cheng-Hao Liu, Marcin Sendera, Siamak Ravanbakhsh, Gauthier Gidel, Yoshua Bengio, Nikolay Malkin, and Alexander Tong. Iterated denoising energy matching for sampling from boltzmann densities, 2024. URL <https://arxiv.org/abs/2402.06121>.

Sina Alemohammad, Josue Casco-Rodriguez, Lorenzo Luzi, Ahmed Imtiaz Humayun, Hossein Babaei, Daniel LeJeune, Ali Siahkoohi, and Richard G Baraniuk. Self-consuming generative models go mad. International Conference on Learning Representations (ICLR), 2024a.

Sina Alemohammad, Ahmed Imtiaz Humayun, Shruti Agarwal, John Collomosse, and Richard Baraniuk. Self-improving diffusion models with synthetic data. *arXiv preprint arXiv:2408.16333*, 2024b.

Brian DO Anderson. Reverse-time diffusion equation models. *Stochastic Processes and their Applications*, 12(3):313–326, 1982.

Weimin Bai, Yifei Wang, Wenzheng Chen, and He Sun. An expectation-maximization algorithm for training clean diffusion models from corrupted observations. In *Proceedings of the 38th International Conference on Neural Information Processing Systems*, NIPS ’24, Red Hook, NY, USA, 2025. Curran Associates Inc. ISBN 9798331314385.

Kevin Black, Michael Janner, Yilun Du, Ilya Kostrikov, and Sergey Levine. Training diffusion models with reinforcement learning. *arXiv preprint arXiv:2305.13301*, 2023.

Ashish Bora, Eric Price, and Alexandros G. Dimakis. AmbientGAN: Generative models from lossy measurements. In *International Conference on Learning Representations*, 2018. URL <https://openreview.net/forum?id=Hy7fDog0b>.

Nicholas Carlini, Jamie Hayes, Milad Nasr, Matthew Jagielski, Vikash Sehwag, Florian Tramèr, Borja Balle, Daphne Ippolito, and Eric Wallace. Extracting training data from diffusion models. In *Proceedings of the 32nd USENIX Conference on Security Symposium*, SEC ’23, USA, 2023. USENIX Association. ISBN 978-1-939133-37-3.

Hong-Bin Chen, Sinho Chewi, and Jonathan Niles-Weed. Dimension-free log-sobolev inequalities for mixture distributions. *Journal of Functional Analysis*, 281(11):109236, 2021.

Thomas A Courtade and Edric Wang. Subadditivity of the log-sobolev constant on convolutions. *arXiv preprint arXiv:2508.19648*, 2025.

Giannis Daras, Kulin Shah, Yuval Dagan, Aravind Gollakota, Alex Dimakis, and Adam Klivans. Ambient diffusion: Learning clean distributions from corrupted data. In A. Oh, T. Naumann, A. Globerson, K. Saenko, M. Hardt, and S. Levine (eds.), *Advances in Neural Information Processing Systems*, volume 36, pp. 288–313. Curran Associates, Inc., 2023. URL https://proceedings.neurips.cc/paper_files/paper/2023/file/012af729c5d14d279581fc8a5db975a1-Conference.pdf.

Giannis Daras, Alexandros G. Dimakis, and Constantinos Daskalakis. Consistent diffusion meets tweedie: training exact ambient diffusion models with noisy data. In *Proceedings of the 41st International Conference on Machine Learning*, ICML’24. JMLR.org, 2024.

Giannis Daras, Yeshwanth Cherapanamjeri, and Constantinos Costis Daskalakis. How much is a noisy image worth? data scaling laws for ambient diffusion. In *The Thirteenth International Conference on Learning Representations*, 2025a. URL <https://openreview.net/forum?id=qZwtPEw2qN>.

Giannis Daras, Jeffrey Ouyang-Zhang, Krithika Ravishankar, William Daspit, Costis Daskalakis, Qiang Liu, Adam Klivans, and Daniel J. Diaz. Ambient proteins: Training diffusion models on low quality structures. *bioRxiv*, 2025b. doi: 10.1101/2025.07.03.663105. URL <https://www.biorxiv.org/content/early/2025/07/05/2025.07.03.663105>.

Giannis Daras, Adrian Rodriguez-Munoz, Adam Klivans, Antonio Torralba, and Constantinos Daskalakis. Ambient diffusion omni: Training good models with bad data. *arXiv preprint arXiv:2506.10038*, 2025c.

Justas Dauparas, Ivan Anishchenko, Nathaniel Bennett, Hua Bai, Robert J Ragotte, Lukas F Milles, Basile IM Wicky, Alexis Courbet, Rob J de Haas, Neville Bethel, et al. Robust deep learning-based protein sequence design using proteinmpnn. *Science*, 378(6615):49–56, 2022.

Alexander Denker, Shreyas Padhy, Francisco Vargas, and Johannes Hertrich. Iterative importance fine-tuning of diffusion models, 2025. URL <https://arxiv.org/abs/2502.04468>.

Prafulla Dhariwal and Alex Nichol. Diffusion models beat gans on image synthesis, 2021. URL <https://arxiv.org/abs/2105.05233>.

Elvis Dohmatob, Yunzhen Feng, Pu Yang, Francois Charton, and Julia Kempe. A tale of tails: Model collapse as a change of scaling laws. *arXiv preprint arXiv:2402.07043*, 2024.

Carles Domingo-Enrich, Michal Drozdal, Brian Karrer, and Ricky TQ Chen. Adjoint matching: Fine-tuning flow and diffusion generative models with memoryless stochastic optimal control. *arXiv preprint arXiv:2409.08861*, 2024.

Bradley Efron. Tweedie’s formula and selection bias. *Journal of the American Statistical Association*, 106(496):1602–1614, 2011.

Yunzhen Feng, Elvis Dohmatob, Pu Yang, Francois Charton, and Julia Kempe. Beyond model collapse: Scaling up with synthesized data requires verification. *arXiv preprint arXiv:2406.07515*, 2024.

Damien Ferbach, Quentin Bertrand, Avishek Joey Bose, and Gauthier Gidel. Self-consuming generative models with curated data provably optimize human preferences. *arXiv preprint arXiv:2407.09499*, 2024.

Samir Yitzhak Gadre, Gabriel Ilharco, Alex Fang, Jonathan Hayase, Georgios Smyrnis, Thao Nguyen, Ryan Marten, Mitchell Wortsman, Dhruba Ghosh, Jieyu Zhang, Eyal Orgad, Rahim Entezari, Giannis Daras, Sarah M Pratt, Vivek Ramanujan, Yonatan Bitton, Kalyani Marathe, Stephen Mussmann, Richard Vencu, Mehdi Cherti, Ranjay Krishna, Pang Wei Koh, Olga Saukh, Alexander Ratner, Shuran Song, Hannaneh Hajishirzi, Ali Farhadi, Romain Beaumont, Sewoong Oh, Alex Dimakis, Jenia Jitsev, Yair Carmon, Vaishaal Shankar, and Ludwig Schmidt. Dat-accomp: In search of the next generation of multimodal datasets. In *Thirty-seventh Conference on Neural Information Processing Systems Datasets and Benchmarks Track*, 2023. URL <https://openreview.net/forum?id=dVaWCDMBof>.

Nate Gillman, Michael Freeman, Daksh Aggarwal, Chia-Hong Hsu, Calvin Luo, Yonglong Tian, and Chen Sun. Self-correcting self-consuming loops for generative model training. *arXiv preprint arXiv:2402.07087*, 2024.

Sachin Goyal, Pratyush Maini, Zachary C Lipton, Aditi Raghunathan, and J Zico Kolter. Scaling laws for data filtering–data curation cannot be compute agnostic. In *Proceedings of the IEEE/CVF Conference on Computer Vision and Pattern Recognition*, pp. 22702–22711, 2024.

Ryuichiro Hataya, Han Bao, and Hiromi Arai. Will large-scale generative models corrupt future datasets? In *Proceedings of the IEEE/CVF International Conference on Computer Vision*, pp. 20555–20565, 2023.

Tom Henighan, Jared Kaplan, Mor Katz, Mark Chen, Christopher Hesse, Jacob Jackson, Heewoo Jun, Tom B Brown, Prafulla Dhariwal, Scott Gray, et al. Scaling laws for autoregressive generative modeling. *arXiv preprint arXiv:2010.14701*, 2020.

Jonathan Ho and Tim Salimans. Classifier-free diffusion guidance. *arXiv preprint arXiv:2207.12598*, 2022.

Jonathan Ho, Ajay Jain, and Pieter Abbeel. Denoising diffusion probabilistic models. In *Proceedings of the 34th International Conference on Neural Information Processing Systems, NIPS '20*, Red Hook, NY, USA, 2020. Curran Associates Inc. ISBN 9781713829546.

Jordan Hoffmann, Sebastian Borgeaud, Arthur Mensch, Elena Buchatskaya, Trevor Cai, Eliza Rutherford, Diego de Las Casas, Lisa Anne Hendricks, Johannes Welbl, Aidan Clark, et al. Training compute-optimal large language models (2022). *arXiv preprint arXiv:2203.15556*, 2022.

Zahra Kadkhodaie, Florentin Guth, Eero P Simoncelli, and Stéphane Mallat. Generalization in diffusion models arises from geometry-adaptive harmonic representations. In *The Twelfth International Conference on Learning Representations*, 2024. URL <https://openreview.net/forum?id=ANvmVS2Yr0>.

Mason Kamb and Surya Ganguli. An analytic theory of creativity in convolutional diffusion models. In *Forty-second International Conference on Machine Learning*, 2025. URL <https://openreview.net/forum?id=ilpL2qACla>.

Jared Kaplan, Sam McCandlish, Tom Henighan, Tom B Brown, Benjamin Chess, Rewon Child, Scott Gray, Alec Radford, Jeffrey Wu, and Dario Amodei. Scaling laws for neural language models. *arXiv preprint arXiv:2001.08361*, 2020.

Tero Karras, Miika Aittala, Timo Aila, and Samuli Laine. Elucidating the design space of diffusion-based generative models. *Advances in neural information processing systems*, 35:26565–26577, 2022.

Varun A. Kelkar, Rucha Deshpande, Arindam Banerjee, and Mark Anastasio. Ambientflow: Invertible generative models from incomplete, noisy measurements. *Transactions on Machine Learning Research*, 2024. ISSN 2835-8856. URL <https://openreview.net/forum?id=txpYITR8oa>.

Alexander Kirillov, Eric Mintun, Nikhila Ravi, Hanzi Mao, Chloe Rolland, Laura Gustafson, Tete Xiao, Spencer Whitehead, Alexander C. Berg, Wan-Yen Lo, Piotr Dollár, and Ross Girshick. Segment anything, 2023. URL <https://arxiv.org/abs/2304.02643>.

Jaakko Lehtinen, Jacob Munkberg, Jon Hasselgren, Samuli Laine, Tero Karras, Miika Aittala, and Timo Aila. Noise2noise: Learning image restoration without clean data. *arXiv preprint arXiv:1803.04189*, 2018.

Jeffrey Li, Alex Fang, Georgios Smyrnis, Maor Ivgi, Matt Jordan, Samir Yitzhak Gadre, Hritik Bansal, Etaish Kumar Guha, Sedrick Keh, Kushal Arora, Saurabh Garg, Rui Xin, Niklas Muenighoff, Reinhard Heckel, Jean Mercat, Mayee F Chen, Suchin Gururangan, Mitchell Wortsman, Alon Albalak, Yonatan Bitton, Marianna Nezhurina, Amro Kamal Mohamed Abbas, Cheng-Yu Hsieh, Dhruba Ghosh, Joshua P Gardner, Maciej Kilian, Hanlin Zhang, Rulin Shao, Sarah M Pratt, Sunny Sanyal, Gabriel Ilharco, Giannis Daras, Kalyani Marathe, Aaron Gokaslan, Jieyu Zhang, Khyathi Chandu, Thao Nguyen, Igor Vasiljevic, Sham M. Kakade, Shuran Song, Sujay Sanghavi, Fartash Faghri, Sewoong Oh, Luke Zettlemoyer, Kyle Lo, Alaaeldin El-Nouby, Hadi

Pouransari, Alexander T Toshev, Stephanie Wang, Dirk Groeneveld, Luca Soldaini, Pang Wei Koh, Jenia Jitsev, Thomas Kollar, Alex Dimakis, Yair Carmon, Achal Dave, Ludwig Schmidt, and Vaishaal Shankar. Datacomp-LM: In search of the next generation of training sets for language models. In *The Thirty-eight Conference on Neural Information Processing Systems Datasets and Benchmarks Track*, 2024. URL <https://openreview.net/forum?id=CNWdWn47IE>.

Zeming Lin, Halil Akin, Roshan Rao, Brian Hie, Zhongkai Zhu, Wenting Lu, Nikita Smetanin, Robert Verkuil, Ori Kabeli, Yaniv Shmueli, et al. Evolutionary-scale prediction of atomic-level protein structure with a language model. *Science*, 379(6637):1123–1130, 2023.

Zeyuan Liu, Zhihe Yang, Jiawei Xu, Rui Yang, Jiafei Lyu, Baoxiang Wang, Yunjian Xu, and Xiu Li. Adg: Ambient diffusion-guided dataset recovery for corruption-robust offline reinforcement learning. *arXiv preprint arXiv:2505.23871*, 2025.

Haoye Lu, Qifan Wu, and Yaoliang Yu. Stochastic forward–backward deconvolution: Training diffusion models with finite noisy datasets. In *Forty-second International Conference on Machine Learning*, 2025. URL <https://openreview.net/forum?id=WrWqv3mpQx>.

Gonzalo Martínez, Lauren Watson, Pedro Reviriego, José Alberto Hernández, Marc Juarez, and Rik Sarkar. Towards understanding the interplay of generative artificial intelligence and the internet. In *International Workshop on Epistemic Uncertainty in Artificial Intelligence*, pp. 59–73, 2023.

Chenlin Meng, Robin Rombach, Ruiqi Gao, Diederik Kingma, Stefano Ermon, Jonathan Ho, and Tim Salimans. On distillation of guided diffusion models. In *Proceedings of the IEEE/CVF conference on computer vision and pattern recognition*, pp. 14297–14306, 2023.

Nick Moran, Dan Schmidt, Yu Zhong, and Patrick Coady. Noisier2noise: Learning to denoise from unpaired noisy data. In *Proceedings of the IEEE/CVF conference on computer vision and pattern recognition*, pp. 12064–12072, 2020.

Bernt Oksendal. *Stochastic differential equations: an introduction with applications*. Springer Science & Business Media, 2013.

Vishakh Padmakumar and He He. Does writing with language models reduce content diversity? In *The Twelfth International Conference on Learning Representations*, 2024. URL <https://openreview.net/forum?id=Feiz5HtCD0>.

William Peebles and Saining Xie. Scalable diffusion models with transformers. In *Proceedings of the IEEE/CVF international conference on computer vision*, pp. 4195–4205, 2023.

Mihir Prabhudesai, Mengning Wu, Amir Zadeh, Katerina Fragkiadaki, and Deepak Pathak. Diffusion beats autoregressive in data-constrained settings. *arXiv preprint arXiv:2507.15857*, 2025.

François Rozet, Gérôme Andry, Francois Lanusse, and Gilles Louppe. Learning diffusion priors from observations by expectation maximization. In *The Thirty-eighth Annual Conference on Neural Information Processing Systems*, 2024. URL <https://openreview.net/forum?id=7v88Fh6iSM>.

Chitwan Saharia, William Chan, Saurabh Saxena, Lala Li, Jay Whang, Emily L Denton, Kamyar Ghasemipour, Raphael Gontijo Lopes, Burcu Karagol Ayan, Tim Salimans, et al. Photorealistic text-to-image diffusion models with deep language understanding. *Advances in neural information processing systems*, 35:36479–36494, 2022.

Tim Salimans and Jonathan Ho. Progressive distillation for fast sampling of diffusion models. *arXiv preprint arXiv:2202.00512*, 2022.

Mohamed El Amine Seddik, Swei-Wen Chen, Soufiane Hayou, Pierre Youssef, and Merouane Abdellkader DEBBAH. How bad is training on synthetic data? a statistical analysis of language model collapse. In *First Conference on Language Modeling*, 2024. URL <https://openreview.net/forum?id=t3z6U1V09o>.

Vikash Sehwag, Xianghao Kong, Jingtao Li, Michael Spranger, and Lingjuan Lyu. Stretching each dollar: Diffusion training from scratch on a micro-budget. In *Proceedings of the Computer Vision and Pattern Recognition Conference*, pp. 28596–28608, 2025.

Kulin Shah, Alkis Kalavasis, Adam Klivans, and Giannis Daras. Does generation require memorization? creative diffusion models using ambient diffusion. In *Forty-second International Conference on Machine Learning*, 2025. URL <https://openreview.net/forum?id=GGPM0z3dhU>.

Piyush Sharma, Nan Ding, Sebastian Goodman, and Radu Soricut. Conceptual captions: A cleaned, hypernymed, image alt-text dataset for automatic image captioning. In Iryna Gurevych and Yusuke Miyao (eds.), *Proceedings of the 56th Annual Meeting of the Association for Computational Linguistics (Volume 1: Long Papers)*, pp. 2556–2565, Melbourne, Australia, July 2018. Association for Computational Linguistics. doi: 10.18653/v1/P18-1238. URL <https://aclanthology.org/P18-1238/>.

Noam Shazeer, Azalia Mirhoseini, Krzysztof Maziarz, Andy Davis, Quoc Le, Geoffrey Hinton, and Jeff Dean. Outrageously large neural networks: The sparsely-gated mixture-of-experts layer. *arXiv preprint arXiv:1701.06538*, 2017.

Ilia Shumailov, Zakhar Shumaylov, Yiren Zhao, Nicolas Papernot, Ross Anderson, and Yarin Gal. Ai models collapse when trained on recursively generated data. *Nature*, 631(8022):755–759, 2024.

Jascha Sohl-Dickstein, Eric Weiss, Niru Maheswaranathan, and Surya Ganguli. Deep unsupervised learning using nonequilibrium thermodynamics. In Francis Bach and David Blei (eds.), *Proceedings of the 32nd International Conference on Machine Learning*, volume 37 of *Proceedings of Machine Learning Research*, pp. 2256–2265, Lille, France, 07–09 Jul 2015. PMLR. URL <https://proceedings.mlr.press/v37/sohl-dickstein15.html>.

Gowthami Somepalli, Vasu Singla, Micah Goldblum, Jonas Geiping, and Tom Goldstein. Diffusion art or digital forgery? investigating data replication in diffusion models. In *Proceedings of the IEEE/CVF conference on computer vision and pattern recognition*, pp. 6048–6058, 2023a.

Gowthami Somepalli, Vasu Singla, Micah Goldblum, Jonas Geiping, and Tom Goldstein. Understanding and mitigating copying in diffusion models. In *Thirty-seventh Conference on Neural Information Processing Systems*, 2023b. URL <https://openreview.net/forum?id=HtMXRGbUMt>.

Jiaming Song, Chenlin Meng, and Stefano Ermon. Denoising diffusion implicit models. *arXiv preprint arXiv:2010.02502*, 2020.

Yang Song and Stefano Ermon. Generative modeling by estimating gradients of the data distribution. In *Advances in Neural Information Processing Systems*, pp. 11895–11907, 2019.

Yang Song, Jascha Sohl-Dickstein, Diederik P Kingma, Abhishek Kumar, Stefano Ermon, and Ben Poole. Score-based generative modeling through stochastic differential equations. In *International Conference on Learning Representations*, 2021. URL <https://openreview.net/forum?id=PxTIG12RRHS>.

Yang Song, Prafulla Dhariwal, Mark Chen, and Ilya Sutskever. Consistency models. 2023.

Charles M Stein. Estimation of the mean of a multivariate normal distribution. *The annals of Statistics*, pp. 1135–1151, 1981.

Keqiang Sun, Junting Pan, Yuying Ge, Hao Li, Haodong Duan, Xiaoshi Wu, Renrui Zhang, Aojun Zhou, Zipeng Qin, Yi Wang, Jifeng Dai, Yu Qiao, Limin Wang, and Hongsheng Li. Journeydb: A benchmark for generative image understanding, 2023. URL <https://arxiv.org/abs/2307.00716>.

Ayush Tewari, Tianwei Yin, George Cazenavette, Semon Reznikov, Josh Tenenbaum, Frédo Durand, Bill Freeman, and Vincent Sitzmann. Diffusion with forward models: Solving stochastic inverse problems without direct supervision. *Advances in Neural Information Processing Systems*, 36:12349–12362, 2023.

Maurice CK Tweedie. Statistical properties of inverse gaussian distributions. i. *The Annals of Mathematical Statistics*, 28(2):362–377, 1957.

Mihaly Varadi, Stephen Anyango, Mandar Deshpande, Sreenath Nair, Cindy Natassia, Galabina Yordanova, David Yuan, Oana Stroe, Gemma Wood, Agata Laydon, et al. Alphafold protein structure database: massively expanding the structural coverage of protein-sequence space with high-accuracy models. *Nucleic acids research*, 50(D1):D439–D444, 2022.

Santosh Vempala and Andre Wibisono. Rapid convergence of the unadjusted langevin algorithm: Isoperimetry suffices. *Advances in neural information processing systems*, 32, 2019.

Zijie J Wang, Evan Montoya, David Munechika, Haoyang Yang, Benjamin Hoover, and Duen Horng Chau. Diffusiondb: A large-scale prompt gallery dataset for text-to-image generative models. *arXiv preprint arXiv:2210.14896*, 2022.

Dongyeop Woo and Sungsoo Ahn. Iterated energy-based flow matching for sampling from boltzmann densities, 2024. URL <https://arxiv.org/abs/2408.16249>.

Jinghui Zhang, Dandan Qiao, Mochen Yang, and Qiang Wei. Regurgitative training: The value of real data in training large language models. *arXiv preprint arXiv:2407.12835*, 2024.

Yasi Zhang, Tianyu Chen, Zhendong Wang, Ying Nian Wu, Mingyuan Zhou, and Oscar Leong. Restoration score distillation: From corrupted diffusion pretraining to one-step high-quality generation. *arXiv preprint arXiv:2505.13377*, 2025.

A Theoretical Results

Lemma 1 (Contractive transformations lead to better learning). *If the mapping function f contracts the TV distance with respect to the underlying true density p_t , i.e., if for any density ϕ it holds that:*

$$d_{\text{TV}}(f \# \phi, p_t) \leq d_{\text{TV}}(\phi, p_t), \quad (9)$$

then, in all cases where Algorithm B is preferable to Algorithm A, according to Criterion 5, Algorithm C is weakly preferable to Algorithm B, and it is strictly preferable if equation 9 is strict.

Proof of Lemma 1: We bound the estimation error made by Algorithms B and C using equation 3. The bounds are the same except that the bound for the error of Algorithm B has an additive term $d_{\text{TV}}(p_t, \tilde{p}_t)$ while the bound for the error of Algorithm C replaces that term with $d_{\text{TV}}(p_t, \tilde{\tilde{p}}_t)$. By definition of \tilde{p}_t and $\tilde{\tilde{p}}_t$, we have:

$$\begin{aligned} d_{\text{TV}}(p_t, \tilde{p}_t) &= \frac{n_2}{n_1 + n_2} d_{\text{TV}}(p_t, q_t), \\ d_{\text{TV}}(p_t, \tilde{\tilde{p}}_t) &= \frac{n_2}{n_1 + n_2} d_{\text{TV}}(p_t, \bar{q}_t) = \frac{n_2}{n_1 + n_2} d_{\text{TV}}(p_t, f \# q_t). \end{aligned}$$

Thus, given equation 9:

$$d_{\text{TV}}(p_t, \tilde{p}_t) \leq d_{\text{TV}}(p_t, \tilde{\tilde{p}}_t),$$

and this inequality becomes strict if equation 9 is strict. Thus, Criterion 5 always weakly prefers Algorithm C to Algorithm B, and the preference is strict if equation 9 is strict. \square

Lemma 2 (Non-Expansion and Contraction under Log-Sobolev). *For $f_{t',t}$ as defined above, it holds, for any f -divergence, that:*

$$D_f(f_{t',t} \# q_t, p_t) \leq D_f(q_t, p_t),$$

Moreover, if i. p_0 is supported in $B(0, R)$ and t is large enough or p_0 satisfies a log-Sobolev inequality with constant C , ii. $\|\frac{\rho_\tau}{p_\tau}\|_\infty \in [1/B, B]$ for some $B > 0$ and all $\tau \in [t, t']$, and iii. $\|\frac{\partial}{\partial \tau} \log p_\tau\|_{L^2(p_\tau)} < A$ for all $\tau \in [t, t']$, then:

$$D_{\text{KL}}(f_{t',t} \# q_t, p_t) \leq (1 - C') D_{\text{KL}}(q_t, p_t),$$

for some $C' < 1$ that depends on A, B and C or R (whichever is applicable) but not the dimension, unless $D_{\text{KL}}(f_{t',t} \# q_t, p_t)$ drops below another absolute constant that depends on A, B and C or R (whichever is applicable) but not the dimension.

Proof of Lemma 2: The first inequality holds by the data-processing inequality. Indeed, consider the noisy channel that takes a sample from q_t (or p_t) and pushes that sample through the noisy channel $f_{t',t}$. By the data-processing inequality the samples at the output of the channel are closer in any f -divergence than the samples at the input of the channel. Moreover, $f_{t',t} \# p_t = p_t$ as the reverse diffusion process was constructed from p_t .

For the second inequality recall that a measure ν satisfies the log-Sobolev inequality (LSI) with a constant $C > 0$ if for all smooth functions g with $\mathbb{E}_\nu[g^2] \leq \infty$:

$$\mathbb{E}_\nu[g^2 \log g^2] - \mathbb{E}_\nu[g^2] \log \mathbb{E}_\nu[g^2] \leq 2C \mathbb{E}_\nu[\|\nabla g\|^2]. \quad (10)$$

It is known that if p_0 is supported on the ball $B(0, R)$, then $p_t = p_0 \circledast \mathcal{N}(0, \sigma_t^2 I)$ satisfies the log-Sobolev inequality with constant $6(4R^2 + \sigma_t^2)e^{\frac{4R^2}{\sigma_t^2}}$ Chen et al. (2021). It is also known that if p_0 satisfies the log-Sobolev inequality with some constant C , then $p_t = p_0 \circledast \mathcal{N}(0, \sigma_t^2 I)$ satisfies the log-Sobolev inequality with constant $C + \sigma_t^2$ Courtade & Wang (2025). In both cases, the measures p_t for t bounded away from 0 satisfy the log-Sobolev inequality for some finite constant. In the second case, this is true for all t . Let us call C' the log-Sobolev constant satisfied by all p_τ , $\tau \in [t, t']$.

Next, recall that we denote by $\rho_\tau(x)$ the distribution of X_τ when we run the backward SDE 7, initialized at $X_{t'} \sim q_{t'}$, for some $t' > t$. For convenience, we define the functions $\tilde{\rho}(\tau) = \rho(t' - \tau)$ and $\tilde{p}(\tau) = p(t' - \tau)$, for all $\tau \in [0, t']$. These distributions satisfy the Fokker-Planck equation:

$$\frac{\partial \tilde{\rho}_\tau}{\partial \tau} = \nabla_x \cdot \left(\tilde{\rho}_\tau \nabla_x \log \frac{\tilde{\rho}_\tau}{\tilde{p}_\tau} \right) \quad (11)$$

Now, for two measures μ, ν on \mathbb{R}^n defined by their probability density functions $\mu(x), \nu(x)$ let us denote by

$$H_\nu(\mu) = \text{KL}(\mu || \nu) \equiv \int_{\mathbb{R}^n} \mu(x) \log \frac{\mu(x)}{\nu(x)} dx,$$

the KL divergence of μ with respect to ν . And let us denote by

$$J_\nu(\mu) = \int_{\mathbb{R}^n} \mu(x) \left\| \nabla \log \frac{\mu(x)}{\nu(x)} \right\|^2 dx,$$

the relative Fisher information of μ with respect to ν . Via a straightforward calculation, generalization the derivation of Vempala & Wibisono (2019) for Langevin diffusion to our non-stationary SDE 7, we obtain the following implication of the Fokker-Planck 11:

$$\frac{d}{d\tau} H_{\tilde{p}_\tau}(\tilde{\rho}_\tau) = -J_{\tilde{p}_\tau}(\tilde{\rho}_\tau) - \int \tilde{\rho}_\tau \frac{\partial}{\partial \tau} \log \tilde{p}_\tau dx. \quad (12)$$

Next we bound the second term of the above identity:

$$\left| \int \tilde{\rho}_\tau \frac{\partial}{\partial \tau} \log \tilde{p}_\tau dx \right| = \left| \int \frac{\tilde{\rho}_\tau}{\tilde{p}_\tau} \frac{\partial}{\partial \tau} \tilde{p}_\tau dx \right| \quad (13)$$

$$= \left| \int \left(\frac{\tilde{\rho}_\tau}{\tilde{p}_\tau} - 1 \right) \frac{\partial}{\partial \tau} \tilde{p}_\tau dx \right| \quad (14)$$

$$= \left| \int \left(\frac{\tilde{\rho}_\tau}{\tilde{p}_\tau} - 1 \right) \tilde{\rho}_\tau \frac{\partial}{\partial \tau} \log \tilde{p}_\tau dx \right| \quad (15)$$

$$\leq \left(\int \left(\frac{\tilde{\rho}_\tau}{\tilde{p}_\tau} - 1 \right)^2 \tilde{p}_\tau dx \right)^{1/2} \left(\int \left(\frac{\partial}{\partial \tau} \log \tilde{p}_\tau \right)^2 \tilde{p}_\tau dx \right)^{1/2} \quad (16)$$

$$= \sqrt{\chi^2(\tilde{\rho}_\tau, \tilde{p}_\tau)} \left(\int \left(\frac{\partial}{\partial \tau} \log \tilde{p}_\tau \right)^2 \tilde{p}_\tau dx \right)^{1/2} \quad (17)$$

$$\leq \sqrt{\chi^2(\tilde{\rho}_\tau, \tilde{p}_\tau)} A \quad (18)$$

where in the second line we used that $\int \frac{\partial}{\partial \tau} \tilde{p}_\tau dx = 0$ (because \tilde{p}_τ is a distribution), in the fourth line we used Cauchy-Schwarz, and in the last line we used our assumption that $\|\frac{\partial}{\partial \tau} \log p_\tau\|_{L^2(p_\tau)} < A$

for all $\tau \in [t, t']$. Next, we relate $\chi^2(\tilde{\rho}_\tau, \tilde{p}_\tau)$ to the KL divergence using our assumption that $\|\frac{\rho_\tau}{p_\tau}\|_\infty \in [1/B, B]$. Namely, it is easy to see that for some B' that only depends on B :

$$\chi^2(\tilde{\rho}_\tau, \tilde{p}_\tau) \leq B' H_{\tilde{p}_\tau}(\tilde{\rho}_\tau).$$

Putting everything together:

$$\frac{d}{d\tau} H_{\tilde{p}_\tau}(\tilde{\rho}_\tau) \leq -J_{\tilde{p}_\tau}(\tilde{\rho}_\tau) + A\sqrt{B' H_{\tilde{p}_\tau}(\tilde{\rho}_\tau)}. \quad (19)$$

Note that, if ν satisfies the log-Sobolev inequality with constant C' , this immediately implies that for all measures μ (by setting $g^2 = \frac{\mu}{\nu}$ in equation 10):

$$H_\nu(\mu) \leq \frac{C'}{2} J_\nu(\mu).$$

Because all measures p_τ satisfy the log-Sobolev inequality with constant C' for all $\tau \in [t, t']$, plugging this into equation 19:

$$\frac{d}{d\tau} H_{\tilde{p}_\tau}(\tilde{\rho}_\tau) \leq -\frac{2}{C'} H_{\tilde{p}_\tau}(\tilde{\rho}_\tau) + A\sqrt{B' H_{\tilde{p}_\tau}(\tilde{\rho}_\tau)}. \quad (20)$$

Denoting by $y(\tau) = \sqrt{H_{\tilde{p}_\tau}(\tilde{\rho}_\tau)}$, the above can be written as:

$$\frac{d}{d\tau} y(\tau) \leq -\frac{1}{C'} y(\tau) + \frac{A\sqrt{B'}}{2}. \quad (21)$$

Integrating, we have that for $\tau \in [0, t' - t]$:

$$y(\tau) \leq e^{-\frac{\tau}{C'}} y(0) + (1 - e^{-\frac{\tau}{C'}}) \frac{AC'\sqrt{B'}}{2}.$$

Recalling that $y(\tau) = \sqrt{H_{\tilde{p}_\tau}(\tilde{\rho}_\tau)} = \sqrt{H_{p_{t'-\tau}}(\rho_{t'-\tau})}$, we have that, for all $\tau \in [t, t']$:

$$\sqrt{H_{p_\tau}(\rho_\tau)} \leq e^{-\frac{t'-\tau}{C'}} \sqrt{H_{p_{t'}}(\rho_{t'})} + (1 - e^{-\frac{t'-\tau}{C'}}) \frac{AC'\sqrt{B'}}{2},$$

which shows that $H_{p_\tau}(\rho_\tau)$ keeps contracting as long as it is larger than $\frac{A^2 C'^2 B'}{4}$. \square

B Additional image results and ablations

B.1 Multiple loops and rate of progress

Table 3: Ablation on number of Dataloops and rate of progress for CIFAR10-32x32 under blur corruption ($\sigma_B = 0.6$). Original $\sigma_{\min} = 1.2$. Metric: FID \downarrow .

Trust rate ρ (noise level)	Ambient Omni (Loop 0)		Loop 1		Loop 2		Loop 3		Loop 4	
	Uncond. FID	Cond. FID	Uncond. FID	Cond. FID	Uncond. FID	Cond. FID	Uncond. FID	Cond. FID	Uncond. FID	Cond. FID
$2^{0.25}$	5.67	4.46	5.44	4.46	5.14	4.14	5.34	4.16	5.49	4.18
$2^{0.50}$	5.67	4.46	5.21	4.26	5.30	4.10	5.26	4.00	5.10	4.00
$2^{1.00}$	5.67	4.46	5.17	4.21	5.31	4.08	5.22	3.91	4.96	3.61
$2^{2.00}$	5.67	4.46	5.14	4.03	4.77	3.53	4.56	3.76	5.08	5.09
$2^{3.00}$	5.67	4.46	4.88	3.98	4.74	3.72	4.65	4.25	5.58	5.68
$2^{4.00}$	5.67	4.46	4.90	4.04	4.76	3.98	4.66	5.19	6.13	8.02
∞	5.67	4.46	5.03	4.14	4.99	4.86	5.86	7.92	8.93	12.69

B.2 Number of posterior samples

A natural ablation to consider is the multiplicity of posterior samplings performed during restoration. Concretely, while for all our experiments in the main paper we did posterior sampling exactly once for each corrupted sample, we can also choose to sample many times from the model using the same corrupted image. As this effectively multiplies the amount of corrupted data in our training set, we duplicate the clean data by the same amount to maintain balance. We see results for training on the multiplied datasets in Table 5 in the case of Blur ($\sigma_B = 0.6$) for the first loop. We observe that for the multiplicities considered (x1, x2, x4), more restorations improve FID.

Table 4: Comparison of restoration methods. FID \downarrow (lower is better). Loop2 restorations. Table 5: Effect of number of posterior samples. Cifar Blur 0.6

Corruption	Restore from scratch	Restore from previous loop	Posterior samples	FID
Blur	$\sigma_B = 0.6$	3.862	x1	4.85
	$\sigma_B = 0.8$	4.481		4.70
JPEG	$q = 25$	4.789	x4	4.52
	$q = 18$	5.260		

B.3 Choice of dataset to restore

In all our experiments in the main paper, we perform the restoration of each DataLoop always starting from the same corrupted samples. In this section, we ablate this choice by comparing to restoring from the previous DataLoop’s restoration i.e. treating them as corrupted samples at a smaller noise level. Table 4 shows conditional FID of the restored dataset in Loop 2 if we restore from scratch vs continuing from the previous loop (Loop 1), in the case of Blur ($\sigma_B = 0.6$). We observe that restoring from the previous loop’s dataset, to the effect of “trusting” the previous loop’s model, actually leads to better conditional FID than restoring from scratch. This shows that errors can accumulate even as models get better from one loop to another.

B.4 Origin of improvement in terms of diffusion times

We also analyze where, in terms of noise times, the improved performance of the Ambient Loops model is coming from compared to the baseline Ambient Omni model. Figure 5 shows average EDM loss curves across different noise times averaged over the entire clean cifar-10 dataset, providing a window of analysis into the per-noise performance of the models. We observe that, for all four corruptions, the Loop1 models are better *for all noise times* than the Omni models. This is initially surprising as Ambient Loops can only facilitate the learning of information present in the dataset (the low-frequencies of the corrupted data), but can do nothing to recover information lost to the corruption (high-frequencies of the corrupted data). The conundrum is explained by the theoretical results: the posterior estimated samples are closer distributionally to the clean samples than the initial blurry samples, and so it is possible to extract more information from them at all noise levels. Indeed, the conditional FID results empirically support this assumption, as seen in 1: the corrupted datasets have conditional FIDs in the 10 to 60 range depending on the severity of the corruption, but the Loop 0 restored datasets all have FIDs below 5.

C ImageNet restoration using a powerful model

In this section, we show we can also use the state-of-the-art image-generation model Flux to “restore” ImageNet, i.e., to improve the quality of ImageNet images without compromising the diversity of the dataset. Specifically, we take the low-quality samples definition from Ambient Omni Daras et al. (2025c), those with CLIP-IQA quality below the 80th percentile, and restore it by first adding noise with $t = 0.3$ ($x_t := (1 - t) \cdot x + t \cdot z$, with $z \sim \mathcal{N}(0, 1)$) and then performing posterior sampling using Flux. As we can see visually in Figure 6, only the quality of the images improved, without altering what is actually depicted in the image. To actually quantify the improvement of quality on ImageNet, we use the CLIP-IQA metric. The results for the original ImageNet and the improved ImageNet are presented in Tables 7 (average CLIP-IQA quality) and 7 (winrate). These metrics, paired with our visuals, show that the quality of the dataset improved.

Table 6: Statistical Summary

Dataset	Mean \pm Std	Min	Max
Original ImageNet	0.7251 ± 0.1572	0.0184	0.9959
Flux-Restored	0.7469 ± 0.1501	0.0265	0.9971

Table 7: Winrate Comparison

Dataset winner	% occurrence
Original ImageNet wins	37.82%
Flux-Restored wins	62.17%

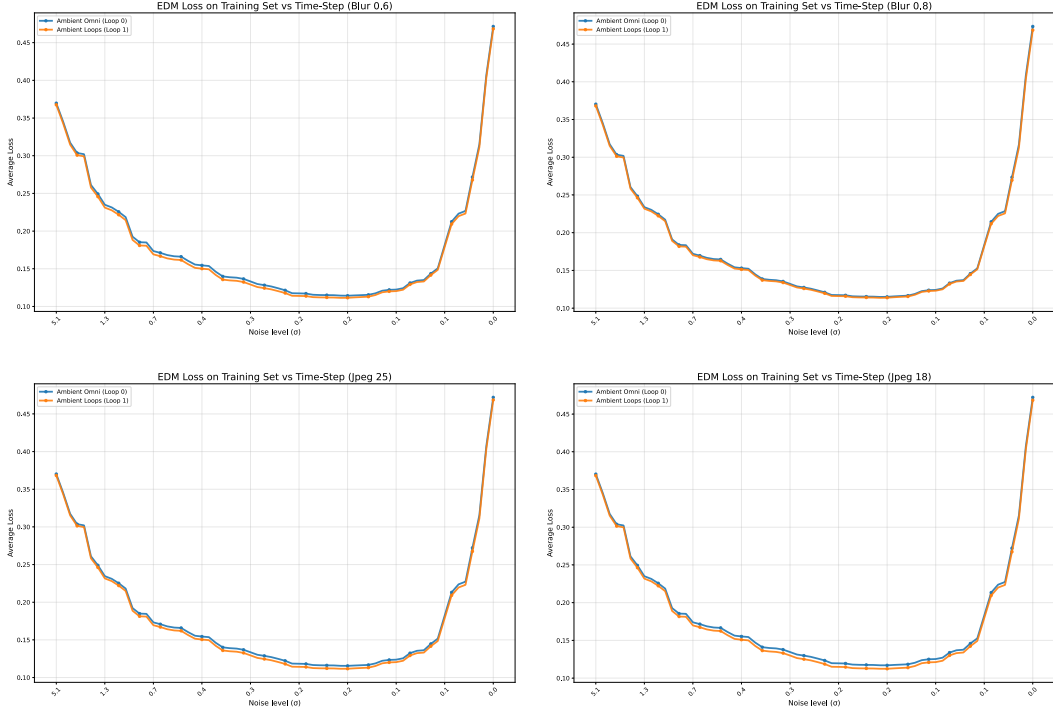


Figure 5: EDM loss vs noise level for Ambient Diffusion Omni Daras et al. (2025c) vs Ambient Loops (Loop 1) models across four corruptions on Cifar-10. Loops models have increased denoising performance *across all* noise levels for all four corruptions.



Figure 6: Examples of ImageNet images well-restored by Flux

D Experimental Details

D.1 Training hyperparameters

For all our controlled experiments in Section 5.1, we use the EDM (Karras et al., 2022) codebase. We provide the full hyperparameters for our models in Table 8.

For our text-to-image experiments, we use the MicroDiffusion (Sehwag et al., 2025) codebase. We start with the checkpoint from the Ambient Diffusion Omni work, available in the following URL:

Hyperparameter	Value
Architecture Type	Diffusion U-net (Song et al., 2020)
# model params	55M
Batch size	512
Maximum training duration (kimg)	200,000
EMA half-life (kimg)	500
EMA ramp-up ratio	0.05
Learning-rate ramp-up (kimg)	10,000

Table 8: Training hyperparameters for our controlled experiments on CIFAR-10.

<https://huggingface.co/giannisdaras/ambient-o>. This model is a Diffusion Transformer (Peebles & Xie, 2023) utilizing Mixture-of-Experts (Shazeer et al., 2017) (MoE) feedforward layers with a total parameter count of $\approx 1.16B$ parameters. We use this checkpoint to restore the DiffDB dataset, after we map it to a noise level $\sigma_{\text{DiffusionDB}} = 2.0$ (see Section 5.2). We finetune the Ambient Omni model on the resulting dataset for $\approx 10M$ images (5000 optimization steps with a batch size of 2048). We provide the full hyperparameters in Table 9.

Hyperparameter	Value
Model Architecture	
VAE	SDXL Base 1.0
Text encoder	DFN5B-CLIP ViT-H/14
Backbone	MicroDiT_XL_2
Latent resolution	64
Image resolution	512
Input channels	4
Precision	bfloat16
Positional interpolation scale	2.0
p_{mean}	0
p_{std}	0.6
Optimization	
Train batch size	2048
Caption drop probability	0.1
Optimizer	AdamW
Learning rate	8×10^{-5}
Weight decay	0.1
ϵ	1×10^{-8}
Betas	(0.9, 0.999)
Gradient clipping (norm)	0.5
Low-precision LayerNorm	amp_bf16
Exponential Moving Average (EMA)	
Smoothing	0.9975
EMA start	2048 kimg
Half-life	None
Training Schedule	
Scheduler	Constant LR
Max duration	10,240 kimg

Table 9: Training hyperparameters for our MicroDiffusion experiment.

For our protein experiments (see Section 5.3), we use the scaled up Genie-2 architecture that the authors of Ambient Proteins (Daras et al., 2025b) proposed. The hyperparameters used to train this model (and our subsequent model) are available in Table 10. We start with the pre-trained model from (Daras et al., 2025b), that is available in the following URL: <https://huggingface.co/jozhang97/ambient-short>. This model was trained on a subset of the AFDB (Varadi et al., 2022) dataset, that is available in the following URL: <https://huggingface.co/datasets/jozhang97/afdb-tm40>. The AFDB dataset contains AlphaFold predictions for protein foldings that vary on accuracy. The Ambient Proteins (Daras et al., 2025b) authors used AlphaFold’s self-reported pLDDT score, to map protein structures to a noise level at which the data can be approximately trusted. In particular, the authors trained their model with 1000

discrete noise levels (cosine diffusion schedule) and the following mapping:

$$\begin{cases} [1, 1000], \text{ pLDDT} \geq 90 \\ [600, 1000], 90 > \text{pLDDT} \geq 80 \\ [900, 1000], 80 > \text{pLDDT} \geq 70. \end{cases} \quad (22)$$

This mapping should be interpreted as follows: proteins that have $\text{pLDDT} \geq 90$ can be used for all diffusion times. Proteins with pLDDT in $[80, 90)$ can be used only for times $[600, 1000]$. Finally, proteins with pLDDT in $[70, 80)$ can be used only for times $[900, 1000]$.

We use the model from (Daras et al., 2025b) to denoise their training set. This results in a new dataset of protein structures that is used for our subsequent training run. Before we proceed with the training phase, we need to quantify how much the noise of the original dataset was reduced. To do so, we experiment with constant increments in pLDDT , and we find that an assumed $+3$ increment in the pLDDT of each denoised protein yields the optimal results. Hence, if a protein before the denoising had a $\text{pLDDT} x$, its new pLDDT after the denoising is assumed to be $x + 3$, and we use the same mapping function (Eq. 22) to convert it to a noise level. With this new dataset and with the training hyperparams detailed in Table 10, we train our model.

Table 10: Training hyperparameters for our proteins experiment.

Hyperparameter	Value
Diffusion	
Number of timesteps	1,000
Noise schedule	Cosine
Model Architecture	
Single feature dimension	384
Pair feature dimension	128
Pair transform layers	8
Triangle dropout	0.25
Structure layers	8
Training	
Optimizer	AdamW
Number of training proteins	196k
Number epochs	200
Warmup iterations	1,000
Total batch size	384
Learning rate	1.0×10^{-4}
Weight decay	0.05
Minimum protein length	20
Maximum protein length	256
Minimum mean pLDDT	70

D.2 Training Computational Requirements

We trained all of our models for the image domain on a cluster of $8 \times \text{H200}$ GPUs. Each CIFAR training (Section 5.1) takes a maximum of 1 day on this compute (200K training kimg), but usually less since models trained on corrupted data converge faster. Our MicroDiffusion (Sehwag et al., 2025) runs (Section 5.2) take only ≈ 7 hours on this compute budget, since we start finetuning from the model of Daras et al. (2025c).

Our protein experiments (Section 5.3) require more compute and we run them on $48 \times \text{H200}$ GPUs. The training takes roughly 12 hours on this compute. This is similar to the compute time needed at the Ambient Proteins (Daras et al., 2025b) paper.

D.3 Restoration Computational Requirements

To run each loop of our algorithm, we need to perform a restoration (i.e. denoising) of the existing dataset. For our CIFAR-10 experiments, the denoising takes ≤ 10 minutes on $8 \times \text{H200}$ GPUs.

This number refers to a full denoising and it is usually faster since we only need to do a partial denoising each time. Restoration time becomes significant for our MicroDiffusion experiments since the dataset is much larger. In particular, restoring the whole Diffusion DB requires 4 days on $48 \times H200$ GPUs. In practice, we only run it for 1 day on the same hardware since the finetuning stage only runs for 1/4th of an epoch and hence we only need to restore 1/4th of DiffusionDB. The restoration cost is also significant for our protein results. Restoration takes roughly 28 hours on $48 \times H200$ GPUs (compared to the 12 hours needed for training). The reason for this overhead is that denoising with posterior sampling requires multiple steps for a single datapoint. This overhead can be reduced by using one step or few-step variants of diffusion models, but we leave this direction for future work.

D.4 Evaluation pipeline

In this subsection we provide some details regarding our evaluation pipeline.

Controlled Experiments. All our controlled experiments are performed on CIFAR-10. CIFAR-10 consists of 50,000 images at 32×32 resolution. For all our experiments, we keep 10% of the training set untouched (i.e. 5000 clean images) and we synthetically corrupt the rest using the different corruption models studied in the paper.

When we compute FID, we always compute it *with respect to the full uncorrupted CIFAR-10*. This allows to truly access whether the model learned the clean distribution and not the distribution after the corruption. To compute FID, we follow standard practice and we generate 50,000 images with the trained model. To estimate the statistical significance of the results, we compute FID 3 times starting with a different generation seed each time. The standard deviations that are reported in Table 1 capture the variability across different FID computations. To find the best obtained FID, we evaluate different checkpoints throughout the training and we report results for the checkpoint that obtained the best mean FID across the three different seeds.

Regarding sampling hyperparameters, we adopt the sampling scheme of the EDM (Karras et al., 2022) paper and we keep all the sampling parameters fixed across different experiments. In particular, we use a sampling budget of 35 Network Function Evaluations (NFEs) and we follow a deterministic sampler using the second order Heun’s discretization method. It is possible that additional benefits could be obtained by tuning separately the sampling hyperparameters for each run.

Text-to-image experiments. For our text-to-image results, we report zero-shot FID on the COCO2014 validation split, following the evaluation protocol of Sehwag et al. (2025). In particular, we generate 30K thousand images using random prompts from the COCO 2014 validation set and we measure the distribution similarity between real and synthetic samples using FID. During our sampling, we use classifier-freee guidance (Ho & Salimans, 2022), i.e., our denoising prediction is formed using a linear combination of the unconditional and conditional prediction of the model, as follows:

$$\hat{x}_0 = (1 + w)h_\theta(x_t, t, c) - wh_\theta(x_t, t, \emptyset), \quad (23)$$

where w controls the guidance strength. We fix $w = 1.5$ for our COCO evaluations. Our sampling budget is 30 NFEs and, similar to our controlled experiments on CIFAR, we use a second-order deterministic sampler based on Heun’s method.

E Noisy dataset formation

Throughout the paper, we assumed access to some dataset $\mathcal{D}_0 = \{(x_{t_i}, t_i)\}_{i=1}^N$ of datapoints x_{t_i} corrupted with additive gaussian noise of variance $\sigma^2(t_i)$. However, in our experiments we deal with points that have been corrupted in various forms beyond additive gaussian noise. In this section of the appendix, we clarify how we transform a dataset of arbitrarily corrupted points into a dataset of points corrupted with additive gaussian noise. The methodology described here is from the paper Ambient Diffusion Omni Daras et al. (2025c). We summarize the main points of the framework here to ensure our paper self-contained. The actual setting studied is the following: there is a dataset $D_h = \{x_{0i}\}_{i=1}^{n_1}$ of high-quality points x_{0i} sampled according to some target distribution p_0 . There is also a dataset $D_l = \{y_{0i}\}_{i=1}^{n_2}$ of potentially low-quality or out-of-distribution points sampled from some other distribution q_0 . For notation purposes, we use the r.v. X_t to denote a point from p_t and

Y_t to denote a point from q_t . Ambient Omni uses D_h as a reference set in order to annotate the points in D_l i.e. to assign a diffusion time t_i to each point y_{0i} from D_l . In particular, the dataset D_0 that is assumed in our setting is formed by concatenating the dataset D_h with a noisy version of D_l denoted by $D'_l = \{(y_{0i} + \sigma(t_i)Z, t_i)\}_{i=1}^{n_2}$ where $Z \sim \mathcal{N}(0, I_d)$. The rest of the discussion focuses on how these annotation noise levels t_i are decided. The authors of (Daras et al., 2025c) propose two ways to perform the annotation:

- Fixed sigma: With this method, all the points in D_l are assigned to the same noise level $\sigma(t_n)$. This noise level is selected such that the TV distance $\text{TV}(p_{t_n}, q_{t_n}) < \epsilon$ for some threshold $\epsilon > 0$. In practice, the value $\sigma(t_n)$ is tuned as a hyper-parameter to achieve optimal validation performance. This value can also be estimated using a classifier, as explained below.
- Time-dependent classifier: In this method, each point in D_l is assigned its own noise level $\sigma(t_i)$. To do so, we first train a time-dependent classifier (Dhariwal & Nichol, 2021) $c_\theta^*(W_t, t)$ that tries to estimate whether a point W_t came from the distribution p_t (label 1) or q_t (label 0), where the r.v.

$$W_t = \begin{cases} X_t & \text{with probability 0.5} \\ Y_t & \text{with probability 0.5} \end{cases}$$

. The classifier is trained with cross-entropy loss trying to predict 1 for points coming from p_t and 0 for points coming from q_t . Simply put, this classifier is trained to distinguish between points from the high-quality and low-quality distributions under noise. Once this classifier is trained, we can use it to annotate points in D_l . In particular, we can assign to each point the minimal diffusion time t_i for which the classifier becomes approximately confused. Formally, for a point y_{0i} in D_l we assign the time $t_i = \inf_t \mathbb{E}_{Z \sim N(0, I_d)}[c_\theta^*(y_{0i} + \sigma(t)Z, t)] \geq \frac{1}{2} - \epsilon$. This classifier can also be used to assign a noise level for the entire dataset (see the above fixed sigma section) by finding the minimal noise level t_n for which the validation accuracy of the classifier is $\leq \frac{1}{2} + \epsilon$.

To avoid the complexities of training classifiers, we use the fixed sigma method for all experiments. However, all of our findings naturally extend to the case of per-data point noise levels.

Now that the set-up has been explained, we need to clarify where do these sets D_h and D_l come from in our experiments, and how the fixed sigma value is decided. For our controlled experiments on Cifar-10, D_h is simply a random 10% of the dataset, and D_l is the remaining 90% but artificially corrupted with either blurring or JPEG compression. The fixed sigma value is obtained by doing hyper-parameter search; the small size of cifar permits such extensive optimization. For our text-to-image experiments, D_h contains all the images from the contextual captions, segment anything, and journeyDB datasets, while D_l contains the images from the diffusionDB dataset. The fixed sigma value is set to 2.0; this value is taken directly from the experiments of Ambient Omni Daras et al. (2025c). For our proteins experiments, we can use AlphaFold to assess the quality of each protein in our training set. AlphaFold reports a self-confidence score, pLDDT, that we use as a proxy of quality. D_h contains all the proteins with $\text{pLDDT} > 90$; these proteins are considered our high-quality data. Proteins with $\text{pLDDT} < 90$ are grouped into three low-quality sets; the noise level for each one of them is assigned using the fixed sigma method and hyper-parameter tuning. Please refer to Section F for details about this annotation scheme.

F Proteins Appendix

F.1 Metrics

Backbone-only generative protein models are principally evaluated with two metrics: designability and diversity.

Designability measures the quality of generated proteins. 100 backbones each of lengths 50, 100, 150, 200, and 250 are generated by the model. To assess whether these backbones could actually be made by some sequence, ProteinMPNN Dauparas et al. (2022) is used to generate eight candidate amino acid sequences per backbone. These are then folded back into structures using ESMFold Lin et al. (2023), and if any of these is sufficiently close to the original backbone ($\text{RMSD} < 2 \text{ \AA}$), the backbone is considered designable. Designability is then defined as the percentage of generated backbones which are designable.

Diversity measures whether a set of generated structures is highly redundant or if it contains a wide array of meaningfully different proteins. To evaluate diversity, Foldseek is used to cluster the set of designable backbones with a TM-score threshold of 0.5. Diversity is defined as:

$$\text{Diversity} = \frac{\text{Number of Clusters}}{\text{Number of Designable Proteins}}$$

In practice, designability and diversity are at odds. Maximizing diversity typically requires generating less likely structures, some of which will not be designable.

F.2 Additional Results

Table 11: **Designability and diversity for protein structure generation.**

Model	Designability (%↑)	Diversity (↑)
<i>Ambient Proteins</i> (L0, $\gamma = 0.35$)	99.2	0.615
Ambient Loops (L1, $\gamma = 0.35$)	99.0	0.703
Proteina (FS $\gamma = 0.35$)	98.2	0.49
Genie2	95.2	0.59
FoldFlow (base)	96.6	0.20
FoldFlow (stoc.)	97.0	0.25
FoldFlow (OT)	97.2	0.37
FrameFlow	88.6	0.53
RFDiffusion	94.4	0.46
Proteus	94.2	0.22



Figure 7: Example denoising (red) of a noisy version (cyan) of the green protein.

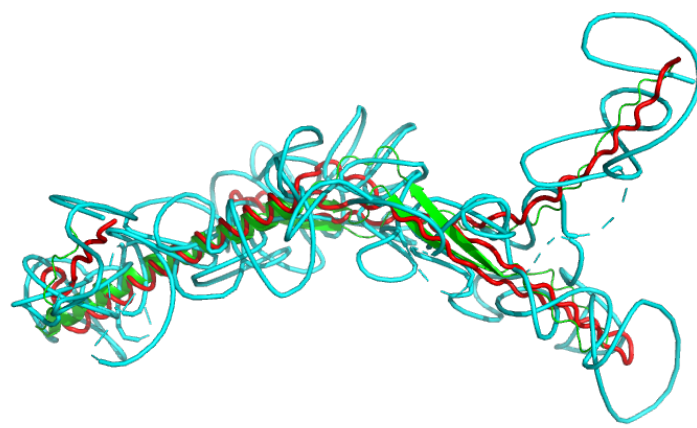


Figure 8: Example denoising (red) of a noisy version (cyan) of the green protein.

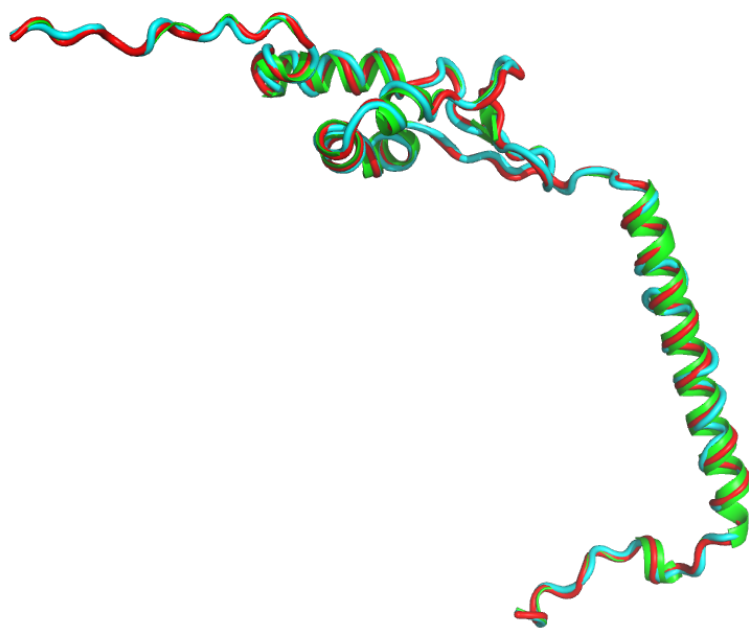


Figure 9: Example denoising (red) of a noisy version (cyan) of the green protein.